Energetic Stability and Interfacial Complexity of $Ti_3C_2T_x$ MXenes Synthesized with HF/HCl and *CoF_2/HCl* as Etching Agents

Cody B. Cockreham [a,b,c], Vitaliy G. Goncharov [a,c,d], Ellis Hammond-Pereira [b], Margaret E. Reece [a,d], Andrew C. Strzelecki [a,c,d,e], Wenqian Xu [f], Steven R. Saunders [b,d,g], Hongwu Xu [c,h], Xiaofeng Guo [a,d,e], Di Wu [a,b,d,e,]*

[a] Alexandra Navrotsky Institute for Experimental Thermodynamics, Washington State University, Pullman, Washington 99164, United States

[b] Voiland School of Chemical Engineering and Bioengineering, Washington State University, Pullman, Washington 99164, United States

[c] Earth and Environmental Sciences Division, Los Alamos National Laboratory, New Mexico 87545, United States

[d] Department of Chemistry, Washington State University, Pullman, Washington 99164, United States

[e] Materials Science and Engineering, Washington State University, Pullman, Washington 99164, United States

[f] X-ray Science Division, Argonne National Laboratory, Advanced Photon Source, Lemont, IL 60438, United States

[g] School of Food Science, Washington State University, Pullman, Washington 99164, United States

[h] School of Molecular Sciences, Arizona State University, Tempe, Arizona 85281, United States

Corresponding Author:

Di Wu, d.wu@wsu.edu

Abstract

MXenes are ultra-thin two-dimensional layered early-transition metal carbides and nitrides with potential applications in various emerging technologies, such as energy storage, water purification, and catalysis. MXenes are synthesized from the parent MAX phase with different etching agents (HF or fluoride salts with a strong acid) by selectively removing a more weakly bound crystalline layer of Al or Ga replaced by surface groups (-O, -F, -OH, etc.). $Ti_3C_2T_x$ MXene synthesized by CoF_2/HCl etching has layered heterogeneity due to intercalated Al^{3+} and Co^{2+} that act as pillars for interlayer spacings. This study investigates the impacts of etching environments on the compositional, interfacial, structural, and thermodynamic properties of $Ti_3C_2T_x$ MXenes. Specifically, compared with HF/HCl etching, CoF_2/HCl treatment leads to a $Ti_3C_2T_x$ MXene with a broader distribution of interlayer distances, increased number of intercalated cations, and decreased degree of hydration. Moreover, we determine the enthalpies of formation at 25 °C ($\Delta H_{f,25°C}$) of $Ti_3C_2T_x$ MXenes etched with CoF_2/HCl, $\Delta H_{f,25°C}$ = –1891.7 ± 35.7 kJ/mol Ti_3C_2, and etched with HF/HCl, $\Delta H_{f,25°C}$ = –1978.2 ± 35.7 kJ/mol Ti_3C_2, using high-temperature oxidation drop calorimetry. These energetic data are discussed and compared with experimentally derived and computationally predicted values to elucidate the effects of intercalants and surface groups of MXenes. We find that MXenes with intercalated metal cations has a less exothermic $\Delta H_{f,25°C}$ from an increase in the interlayer space and dimension heterogeneity and a decrease in the degree of hydration leading to reduced layer–layer van der Waals interactions and weakened hydration effects applied on the MXene layers. The outcomes of this study further our understanding of MXene's energetic–structure–interfacial property relationships.

Introduction

MXenes are a family of two-dimensional layered materials with a "magazine" style morphology. [1] These ultra-thin ceramics present great potential in various applications, especially in electrochemical energy storage. [2–5] Compositionally, MXenes are early transition metal carbides and nitrides in the form of $M_{n+1}X_nT_x$, where M is an early transition metal such as Ti or V, X is C or N, and T_x represents the capping end-groups (-F, -OH, =O, etc.) determined primarily by the synthesis environment. [6,7] In addition, MXenes can host intercalants, especially tightly confined interlayer water and ions, which defines its energy storage mechanism. [8–13] $Ti_3C_2T_x$ MXene is the most widely investigated of its family and acts as a representative system. $Ti_3C_2T_x$ MXene was originally synthesized by selective etching of the Al layer of stratified Ti_3AlC_2 with hydrofluoric acid (HF). [14] Since, new synthesis methodologies have arisen. Specifically, HF formation is created indirectly by combining strong acids with fluoride salts. For example, LiF/HCl etching is prevalent and has been found to feature a gentle etching mechanism allowing large MXene flakes. [10,15] Other salts have also been used with HCl, such as NaF, KF, and FeF_3. [16,17] Recently, we reported a new method in which CoF_x/HCl (x = 2 or 3) was used as the etching agent. [18] Variation in the etching agent and/or environment leads to significantly different surface chemistry, type, and concentration of intercalants, and MXene structural features, this, in turn, affects its properties, such as thermal stability, conductivity, capacitance, etc. [19–24] The fluoride content and ionic strength in solution control the formation of AlF_3 precipitated as $AlF_3{\cdot}3H_2O$, a common impurity. [15,18,25,26]

We recently reported the unexpected structural heterogeneity of $Ti_3C_2T_x$ MXene etched with CoF_2/HCl, which has low $AlF_3{\cdot}3H_2O$ impurity. [27] We found that CoF_2/HCl etching leads to $Ti_3C_2T_x$ MXene with pillared layers. Removal of interlayer confined molecular water revealed two

distinctive layering systems, specifically, (*i*) typical $Ti_3C_2T_x$ MXene layers reduced the interlayer spacing upon water removal, and (*ii*) pillared $Ti_3C_2T_x$ MXene layers that retained their open and large interlayer spacing even after deintercalation of water. [27] Such structural heterogeneity is probably due to the presence of trapped/intercalated Al^{3+} and/or Co^{2+} species in the interlayer space because of the high diffusion barrier from the strong ionic strength of the CoF_2/HCl etching environment. However, the energetics of formation and intercalant–layer guest–host interactions, which govern the formation of this unique $Ti_3C_2T_x$ MXene system featuring heterogeneously pillared layered structures, have not been experimentally investigated.

The thermodynamic stability of $Ti_3C_2T_x$ MXenes synthesized with different etching agents has been studied computationally and experimentally. *Sharma et al.* determined the enthalpy of formation for Ti_3AlC_2 MAX and a $Ti_3C_2T_x$ MXene etched in LiF/HCl using high-temperature oxide melt solution calorimetry. [28] This study confirms that the formation of $Ti_3C_2T_x$ MXene is more exothermic than Ti_3AlC_2 MAX, and highlights the role that surface chemistry plays in the stabilization of Ti_3C_2 MXene layers. Likewise, computational studies predicted the role of termination groups to stabilize the surface. [29–34] These studies provide crucial energetic insights into the thermodynamic stability of MXenes and the surface chemistry of the stacked layers.

Nevertheless, the roles of different interlayer species and the guest–host interfacial chemistry play in determining thermodynamic, structures, and interfacial properties of MXene materials have not been systematically explored. [35–38] There has been progress towards investigating water/ion–layer interactions, yet the energetics of intercalated particle – MXene layer interactions and why they present higher exothermic formation enthalpies from elements than the bulk parent MAX phases after synthesis and high-temperature treatments have not been clearly understood. [11,39–43] In other words, unlocking MXene's full potential requires an improved

understanding of the energetic interplay of intercalants, surface chemistry, and specific layered structures for samples synthesized under different etching conditions and with varied etching agents.

Here, we present a thermochemical investigation into the energetics of formation and intercalates–layer guest–host interactions of MXenes synthesized using CoF_2/HCl and HF/HCl as the etching agents. We have recently reviewed common calorimetric methods to investigate guest–host interactions. [44] In this study, leveraging high-temperature oxidation drop calorimetry, we derive the enthalpies of oxidation and standard enthalpies of formation from elements at 700 °C in the oxygen atmosphere. Further, these new energetic insights into the formation of MXenes under different synthesis conditions were discussed and compared with experimentally measured and computationally predicted values reported in earlier studies.

Experimental Methods

Synthesis of $Ti_3C_2T_x$ MXene by CoF_2/HCl Etching

Ti_3AlC_2 MAX phase was purchased from Luoyang Tongrun Info. Technology Co., Ltd. with a reported mean particle size of ~800 nm. 1.0 g of Ti_3AlC_2 corresponding to 4.3 wt.% was added to 20 mL of 6 M HCl, prepared from 37 wt.% HCl (Sigma-Aldrich) mixed in a 50 mL polypropylene test tube. 1.75 g of CoF_2 (Sigma-Aldrich) corresponding to a CoF_2 to Ti_3AlC_2 molar ratio of 3.6. The solution was mixed for 30 sec using a test tube agitator and then put into the bath-sonicator for 30 min, after which the mixture was heated to 60 °C for 48 hrs. The suspension was washed with copious amounts of deionized water over a vacuum filtration system and left to dry for 12 hrs. The powder was collected and dried overnight in a vacuum at ~ 60 °C.

Synthesis of $Ti_3C_2T_x$ MXene by HF/HCl Etching

1.0 g of Ti_3AlC_2 was introduced to a solution made of 1.6 mL 48 wt.% HF (Sigma-Aldrich), 7 mL of 37 wt.% HCl (Sigma-Aldrich), and 11.4 mL of deionized water. The solution was calculated to contain the same fluoride ions (F^-) and pH as performed in the CoF_2/HCl etching described above. The synthesis and post-synthesis treatments were identical to that of the CoF_2/HCl etched sample.

Compositional Analyses

Inductively coupled plasma–optical emission spectrometry (ICP-OES, Agilent Technologies 5100) was used to determine the quantitative elemental ratios of Ti, Al, and Co within the samples. About 2.0 mg of each powdered sample was dissolved in 50 mL of an acidic aqueous medium (~4% HNO_3) by heating the mixtures overnight at 75 °C. Calibrant stock solutions were prepared through the dilution of ICP standards purchased from Ultra Scientific (Ti) and Inorganic Ventures (Al and Co) in an acidic aqueous solution (adjusted to ~4% HNO_3). Powder X-ray fluorescence was conducted before ICP-OES analysis to estimate the contents of Ti, Al, and Co. The C, H, F, and Cl contents were determined at the Atlantic Microlab, Inc., Norcross, GA. Specifically, the analyses of C and H were performed by combustion using automatic analyzers. F and Cl analyses were carried out by flask combustion followed by ion chromatography. The water content was quantified by thermal analysis, which is described below. The measurements were repeated to ensure accuracy and reproductivity, five times for CoF_2-MXene, and four times HF-MXene. To calculate the sample compositions, first, the measured total C content (Atlantic Microlab) is used as the basis. The cationic stoichiometries of Ti, Al, and Co are derived based on the ICP-OES results. The minor impurity species, $AlF_3 \cdot 3H_2O$ and unreacted Ti_3AlC_2 MAX are determined by quantitative X-ray diffraction (QXRD) with corundum as an internal standard and are subtracted from MXene sample mass. The contents of pure MXene (Ti_3C_2)

with termination functional groups F and Cl are determined with Atlantic Microlab. The OH group content is determined by subtracting H of all H_2O from the total amount of H measured (Atlantic Microlab). The remaining mass is attributed to =O groups. Moreover, according to the synchrotron XRD data, we have not seen any detectable bulk oxide phases such as TiO_2 or Al_2O_3 following synthesis.

Thermal Analysis

Thermogravimetric analysis and differential scanning calorimetry (TG-DSC) were performed on a Netzsch Jupiter STA 449 F1 at a heating rate of 10 °C/min under 50 ml/min oxygen flow. 5 to 10 mg of MXene sample was analyzed in an alumina crucible from 30 to 900 °C. The sensitivity calibrations were performed with sapphire pucks in each environment before the measurement. The H_2O content was determined from TG curves, 7.2 ± 0.3 wt.% (CoF_2-MXene) and 10.8 ± 0.7 wt.% (HF-MXene).

Synchrotron X-ray Diffraction (XRD)

Synchrotron powder XRD was conducted at Sector 17-BM-B of Advanced Photon Source (APS) at Argonne National Laboratory (ANL). The wavelength of the X-ray beam was $\lambda = 0.24099$ Å. The sample's distance to the detector was fixed at 700 mm for the XRD measurements. The MXene sample powders were contained in Kapton capillaries sealed on both sides with epoxy. All collected two-dimensional images were calibrated, masked, and integrated using Dioptas processing software. [45] Lattice parameters of $Ti_3C_2T_x$ MXene were calculated using Bragg's law in the $P6_3/mmc$ [194] space group. [46]

XRD data for quantitative compositional analysis was obtained using a Bruker D8 Advance with Cu Kα radiation ($\lambda = 1.5406$ Å) operated at a scan rate of 1 °/min between 5 and 80°. 20 wt.%

of corundum powder was ground into the MXene powders with acetone using a Brinkmann grinder. Rietveld refinements were performed using *Profex 4.3.5* software with phases from the *Crystallography Open Database*, www.crystallography.net. [47–52] The crystallographic information files (CIFs) of Ti_3AlC_2 MAX (ID: mp-3747) and Ti_3C_2 MXene (ID: mp-1094034) were retrieved from the *Materials Project* online database, www.materialsproject.org. [53] The range of 2θ = 14 to 60 was used for the refinements to reduce difficulties caused by MXene's preferred orientation effects in low 2θs. XRD patterns for the Ti_3AlC_2 MAX phase were obtained with a Rigaku Smartlab with Cu Kα radiation operated at a scan rate of 4 °/min from 5 to 80°. For isothermally treated MXenes, XRD was obtained using a Bruker D8 Advance with Cu Kα radiation operated at a scan rate of 4 °/min in the 2θ range of 5 – 80°.

Transmission Electron Microscopy (TEM)

An FEI Tecnai T20 transmission electron microscope (TEM) using a LaB_6 cathode was operated at 200 kV for imaging. MXene particles were dispersed in ethanol (2 mg MXene/mL ethanol). ~3 µL dispersion was taken and deposited on a 200 mesh formvar/carbon TEM grid. Micrograph analysis was conducted using ImageJ (NIH). [54]

High-Temperature Drop Oxidation Calorimetry

Calorimetric measurements were conducted using a Tian-Calvet twin microcalorimeter, Setaram Alexis-1000. [55–57] Powdered MXene samples were pressed into ~5 mg pellets under an ambient environment using a hand die. Each sample pellet was dropped from room temperature into the calorimetry chamber maintained at 700 °C, where quartz crucibles with pure oxygen flow ~110 mL/min. The heat effects reflect the sample oxidation at the temperature of measurement. The heat effect is integrated over time to derive the enthalpy of oxidation drop ($\Delta H_{ox,700°C}$).

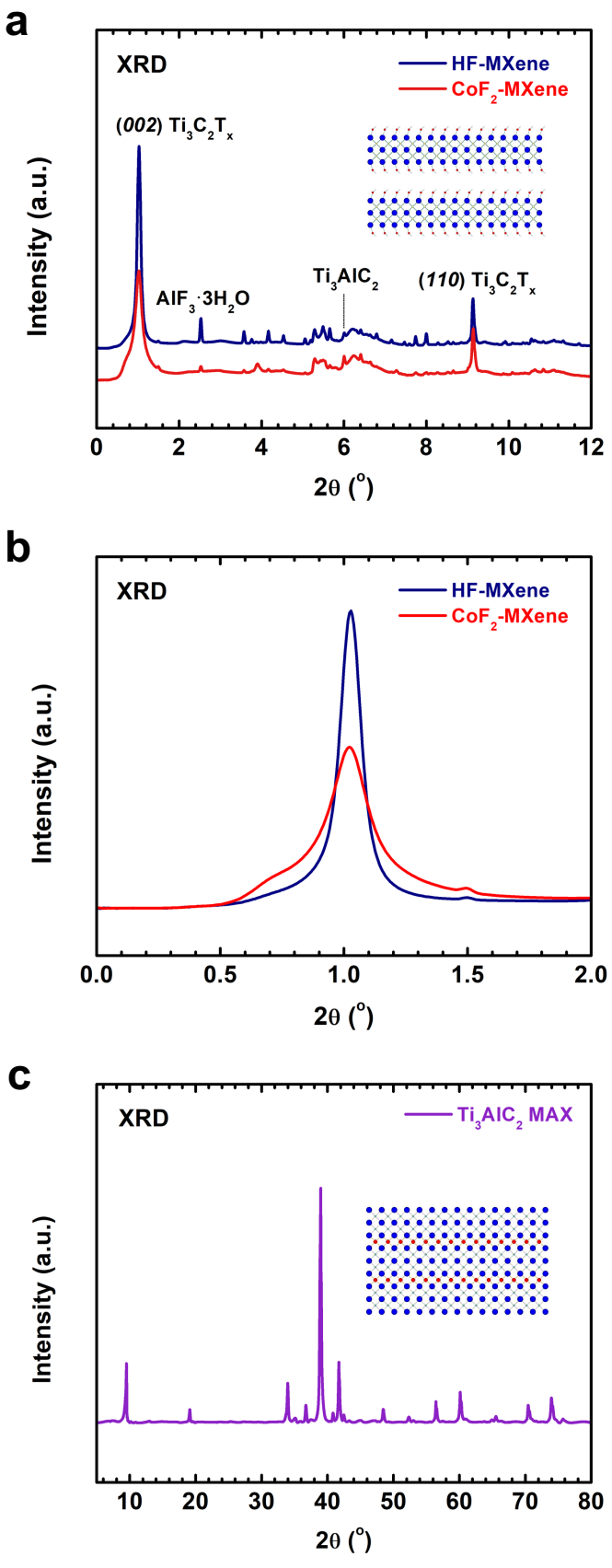

Figure 1. X-ray diffraction (XRD) patterns of CoF_2-MXene and HF-MXene were collected with synchrotron radiation (λ = 0.24099 Å). (**a**) Full XRD patterns and (**b**) low 2θs, showing MXene's (002) peak with a shoulder between 0.5 – 1°. **(c)** The XRD pattern (Cu Kα radiation) of their parent Ti_3AlC_2 MAX phase is also plotted.

Successful oxidation is ensured by heat flux return to baseline. The calorimeter calibration was carried out by using the heat content of α-Al_2O_3 (corundum) powder pellets dropped in an empty crucible. Errors were calculated as the two standard deviations of the mean.

Results and Discussion

We denoted the $Ti_3C_2T_x$ MXene synthesized from the Ti_3AlC_2 MAX phase by etching using CoF_2/HCl and HF/HCl with the same pH and fluoride content as CoF_2-MXene and HF-MXene, respectively. According to the synchrotron X-ray diffraction (XRD) patterns in **Figures 1a** and **b**, both CoF_2-MXene and HF-MXene are confirmed to have a near-complete conversion from MAX to MXene. The benchtop XRD patterns of the Ti_3AlC_2 MAX parent phase are plotted in **Figure 1c**. XRD analysis suggests a minor amount of $AlF_3{\cdot}3H_2O$ residual. The contents of $AlF_3{\cdot}3H_2O$ and unreacted Ti_3AlC_2 MAX are calculated via refinements of XRD patterns (see **Figures S1** and **S2**). The compositions of MXene samples synthesized in this study are summarized in **Table 1**. CoF_2-MXene has a calculated MXene composition of $Ti_3C_2F_{1.05}Cl_{0.09}(OH)_{1.15}O_{3.10}Al_{0.26}Co_{0.03}(H_2O)_{0.76}$ with 0.15 mol $AlF_3{\cdot}3H_2O$ impurity and 0.06 mol Ti_3AlC_2 unreacted MAX phase. HF-MXene has a calculated MXene composition of $Ti_3C_2F_{1.71}Cl_{0.12}(OH)_{1.64}O_{2.51}Al_{0.02}(H_2O)_{0.95}$ with 0.29 mol $AlF_3{\cdot}3H_2O$ impurity and 0.04 mol Ti_3AlC_2 unreacted MAX phase.

Under reaction conditions, in an aqueous solution, F^- etch the Al layer of Ti_3AlC_2 MAX. To balance charges in solution and the surface charges of the functional groups attached to the Ti_3C_2 MXene, a positively charged species must also insert into the interlayer space. Due to the acidic synthesis environment and significantly smaller size of H^+ and greater mobility, H^+ is likely the predominant charge balancing species. From ICP-OES, XRF, and energy dispersive X-ray spectroscopy (EDS not presented here), we find that Co^{2+} is significantly lower in content than

Al^{3+} with very low quantities. The compositional analysis finds that, in our synthesis conditions, the insertion of Co^{2+} into the interlayer space is less preferred than the insertion of H^+ or exchange with recently etched Al^{3+}. This is mostly related to the greater size of the Co^{2+} and its complexes with water, and the energy required to remove the hydration shell of Co^{2+}.

Table 1. Compositions of all as-synthesized samples, including MXenes, $AlF_3{\cdot}3H_2O$ by-product, and unreacted Ti_3AlC_2 MAX.

Sample	Composition
Total CoF_2-MXene sample	$Ti_3C_2F_{1.05}Cl_{0.09}(OH)_{1.15}O_{3.10}Al_{0.26}Co_{0.03}(H_2O)_{0.76}$ + 0.15 $AlF_3{\cdot}3H_2O$ + 0.06 Ti_3AlC_2
Total HF-MXene sample	$Ti_3C_2F_{1.71}Cl_{0.12}(OH)_{1.64}O_{2.51}Al_{0.02}(H_2O)_{0.95}$ + 0.29 $AlF_3{\cdot}3H_2O$ + 0.04 Ti_3AlC_2

As anticipated, we have found that the CoF_2-MXene sample contains cationic species that cannot be ascribed to unreacted Ti_3AlC_2 or bulk $AlF_3{\cdot}3H_2O$, specifically, 0.26 mole of Al^{3+}, 0.03 mole of Co^{2+} per mole of Ti_3C_2. In comparison, HF-MXene has 0.02 mole of Al^{3+} per mole of Ti_3C_2. Typically, the cationic species are intercalated within the interlayer spacing of MXene. Otherwise, they would have been easily removed in the post-synthesis washing. This is in line with our previously reported results. We reported intercalated Al^{3+} species that act as pillaring agents and are "trapped" in the interlayer space post-synthesis and washing treatments. [27] Both CoF_2-MXene and HF-MXene, feature rich interfacial chemistry with complex surface functionalization. This is most likely due to surface attachment past ideal stoichiometry. The speciation of intercalated ion complexes, such as the interlayer AlF_3 species, could also contribute. Surface attachment past stoichiometry is computationally predicted by exergonic attachment of F^- to an already fully terminated $Ti_3C_2O_2$ MXene. [30] Although our samples show more bound surface groups than the ideal stoichiometric surface functionalization ($Ti_3C_2T_x$, $x = 2$), the ratio of surface groups are $O_{0.58}F_{0.19}(OH)_{0.21}Cl_{0.02}$ and $O_{0.42}F_{0.29}(OH)_{0.27}Cl_{0.02}$ for CoF_2-MXene and HF-MXene,

respectively. Only O and F functional groups are predicted to exist in an ambient oxygen environment. [30] However, using a multilevel computational strategy, Gibb's free energy of formation was found to be the lowest with a ratio of surface groups for a $Ti_3C_2T_x$ MXene in a solution with pH = 0 (and an open circuit potential of 0 V) was found to be $O_{0.5}F_{0.25}OH_{0.25}$. [31] Our MXenes, synthesized in a calculated pH of – 0.8, support this prediction with experimental evidence. Here, the low content of Cl functional groups observed is typical in MXene synthesis. Adsorption of Cl as a surface functional group is unlikely due to its lower energy of adsorption compared with that of O, OH, and F. [30] Generally, it is difficult to intercalate anions, and it has been suggested that large anions (Cl, Br, etc.) may be adsorbed to the edges of MXene during synthesis. [9,58]

Table 2. Lattice parameters of the MXenes, determined from synchrotron X-ray diffraction (XRD) patterns.

Sample	Lattice Parameters		
	a (Å)	*c* (Å)	Unit Cell Volume (Å^3)
CoF_2-MXene	3.025	27.011	214.1
HF-MXene	3.027	26.858	213.1

$Ti_3C_2T_x$ MXenes have a hexagonal structure with a $P6_3/mmc$ space group. According to the synchrotron XRD data, the lattice parameters and unit cell volumes were calculated with Bragg's law using the (*002*) and (*110*) peaks (see **Table 2**). Both MXene samples have similar lattice parameters and unit cell volumes, $a = \sim 3$ Å, $c = \sim 27$ Å, and $V = \sim 215$ Å^3. However, interestingly, CoF_2-MXene displays a much broader (*002*) peak compared with that HF-MXene, which is centered at $2\theta = 1°$. The (*002*) plane is representative of the interlayer direction of $Ti_3C_2T_x$ MXene; the broader (*002*) peak of CoF_2-MXene suggests it features a broader distribution of interlayer distances compared with HF-MXene (see **Figure 1b**). HF-MXene has an interlayer distance that

is more uniformly distributed. CoF_2-MXene has a distinct shoulder to the (*002*) peak between 2θ = 0.5 – 1.0°, reflecting the presence of a pillared structure. [27] Using this shoulder at 0.77° to calculate a *c* lattice parameter of 36 Å reveals layering with ultra-large interlayer spacing for CoF_2-MXene. Smaller cations with lower charges, such as Na^+ or K^+, lead to larger interlayer spaces than multivalent cations like Al^{3+} due to their smaller hydration shell, allowing two layers of cations and associated water within an interlayer space. [59] Al^{3+} has been considered an effective pillaring agent by expanding the MXene's interlayer channels and providing greater access for water to pass through when driven by an osmotic gradient. [60] Despite having a portion of larger interlayer spacings, surprisingly, CoF_2-MXene contains less water (0.76 mole H_2O per mole of Ti_3C_2) compared with HF-MXene (0.95 mole H_2O per mole of Ti_3C_2). For the as-made, hydrated MXenes, with similar unit cell volumes and *c* lattice parameters, Al^{3+} and Co^{2+} cations occupy interlayer space in CoF_2-MXene that likely hosts intercalated water in HF-MXene. Our interpretation is supported by the evidence that less water resides in the metal-ion-intercalated $Ti_3C_2T_x$ MXenes. [61] Thus, the pillared heterogeneity of CoF_2-MXene is caused by the intercalation of Al^{3+}, Co^{2+}, and water which modifies the interlayer space. The compositional and structural analyses support this.

Using transmission electron microscopy (TEM), sample morphology was investigated. **Figure 2** shows TEM images with a perspective parallel to the layer-layer stacking. Both samples present the same laminated structure with dense layers and less dense interlayer spaces, and the layers stack tightly. **Figure 2a** displays a few particles loosely attached to the $Ti_3C_2T_x$ MXene particles, which are minor etching residuals described in our previous investigations into the morphology of $Ti_3C_2T_x$ MXene. [18,27] $Ti_3C_2T_x$ is oxidized in the air over long periods, showing these small popcorn-like particles on the surface. [62] Our samples do not show detectable oxidation

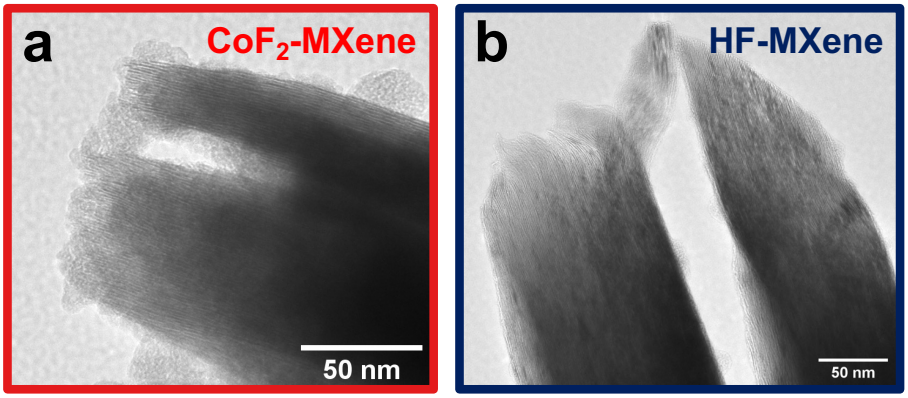

Figure 2. Transmission electron microscopy (TEM) images of (**a**) CoF_2-MXene and (**b**) HF-MXene, oriented in the planar direction so that the layer-layer stacking is observed.

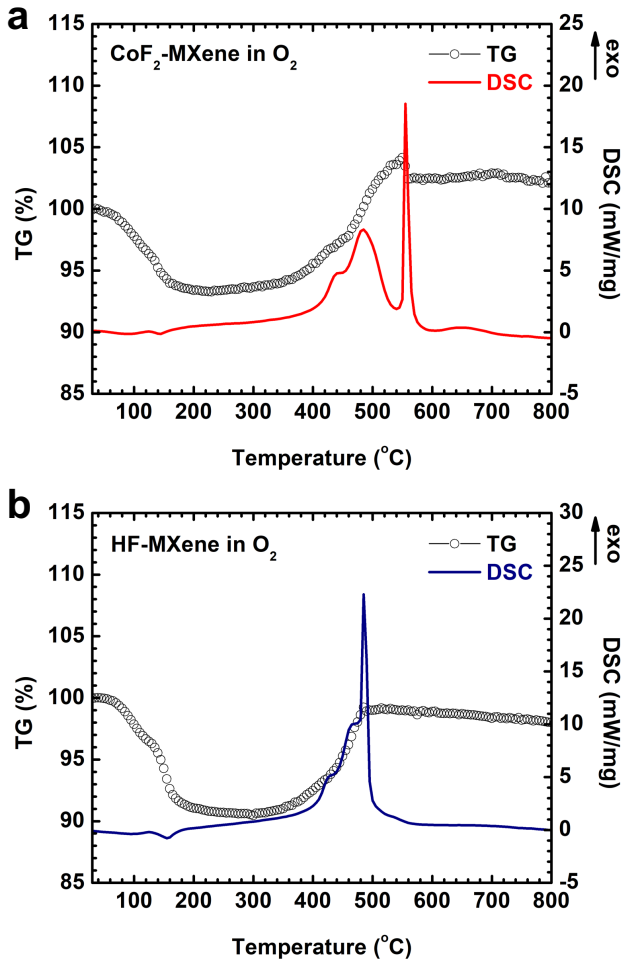

Figure 3. Thermogravimetric analysis – differential scanning calorimetry (TG-DSC) curves of **(a)** CoF_2-MXene and **(b)** HF-MXene in oxygen (50 ml/min) at a scan rate of 10 °C/min.

products compared to those with significant TiO_2 particle growth on their surface. [17] **Figure 2b** highlights $Ti_3C_2T_x$ MXene's mechanical flexibility; the near-edge MXene layers bend like paint-brush bristles. According to the TEM images, CoF_2-MXene and HF-MXene exhibit similar morphological behaviors.

Thermal analysis was performed using TG-DSC in oxygen flow (see **Figure 3**). Both samples present the same behavior. The physisorbed and interlayer confined water molecules are liberated between 100 to 150 °C leading to a broad TG mass loss. The second TG step is associated with a weakly endothermic peak between 150 and 200 °C, suggesting the removal of crystalline water from $AlF_3 \cdot 3H_2O$ as it decomposes to $AlF_3 \cdot 0.5H_2O$. [63] Subsequently, oxidation reactions of C and Ti, occur above 300 °C, suggested by a series of significantly exothermic peaks and continuous mass increase for both samples. Not able to be differentiated here, $AlF_3 \cdot 0.5H_2O$ is expected to decompose to AlF_3 between 277 and 550 °C. [63] More specifically, the first two broad exothermic shoulders and initial weight gain, occurring at ~415 °C and ~450 °C, correspond to oxidation of the Ti outer layers of MXene and oxidation of AlF_3 to Al_2O_3. Here, it is unclear which reaction is associated with which peak due to the significant overlap in the reactions. This agrees well with results from previous studies. [62,63] The -F and -Cl functional groups of the outer layers of Ti are evolved as F_2 and Cl_2. Hydroxyl groups are detached forming H_2O and leaving behind an O. A relatively weak exothermic peak emerges simultaneously as a loss of mass at about 480 °C for CoF_2-MXene and at about 460 °C for HF-MXene. This is associated with the oxidation of innermost layer of Ti of MXene. Eventually, the carbon layers rapidly oxidize (combustion) to CO_2 between 500 and 600 °C (combustion). [69] Above 600 °C and up to 800 °C, the TG and DSC profiles are nearly featureless. We find that MXene and $AlF_3 \cdot 3H_2O$ complete their conversion to oxides below 700 °C.

Successful decomposition to oxide phases at 700 °C was ensured by performing TG-DSC and XRD on MXenes after isothermal treatment in air at 700 °C for 1 hr. TG-DSC measurements show completion of exothermic reactions and mass change at 700 °C, discussed above. The XRD patterns have no evidence of $Ti_3C_2T_x$, Ti_3AlC_2, or AlF_3 phases but do show TiO_2 (anatase >> rutile) and corundum Al_2O_3 (see **Figure 4**). Anatase is the preferred phase formed during the oxidation of $Ti_3C_2T_x$ MXene, so we use anatase as the reference phase in thermochemical cycles. [62] Other studies also support complete oxidation at 700 °C in oxygen or air. For example, in oxygen, $Ti_3C_2T_x$ MXene loses its water and surface groups at 150 °C. Subsequently, Ti and C are oxidized between 150 and 350 °C, evidencing the oxidation reaction completion below 500 °C. [64,65] Since the MXene samples are completely oxidized at 700 °C in oxygen, high-temperature drop oxidation calorimetry is appropriate for the formation enthalpy measurements.

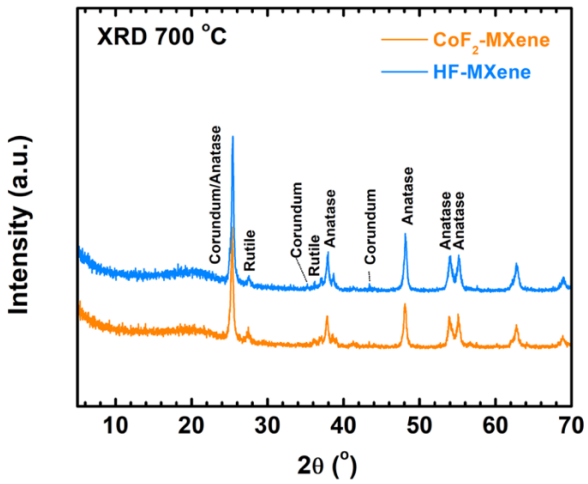

Figure 4. X-ray diffraction (XRD) patterns of CoF_2-MXene and HF-MXene using Cu Kα radiation after isothermal treatment at 700 °C for 1 hr and allowed to naturally cool to room temperature in the furnace over an ~8 hr period.

High-temperature drop oxidation calorimetry was primarily used to investigate the thermodynamics of other carbon materials, including carbon nanotubes, onion-like carbon, nanodiamonds, and metal-organic frameworks. [66–69] Dropping samples from room temperature to

an oxidative environment was used to measure the enthalpic response from heating to 700 °C and oxidation, $\Delta H_{ox,700°C}$. The individual heat effects of drop oxidation calorimetry measurements are summarized in **Table S1**. The total enthalpies of drop oxidation returned $\Delta H_{ox,\ 700°C,\ total} = -2337.3 \pm 34.9$ kJ/mol [$Ti_3C_2F_{1.05}Cl_{0.09}(OH)_{1.15}O_{3.10}Al_{0.26}Co_{0.03}(H_2O)_{0.76} + 0.15\ AlF_3{\cdot}3H_2O + 0.06\ Ti_3AlC_2$] for CoF_2-MXene, and -2279.1 ± 34.8 kJ/mol [$Ti_3C_2F_{1.71}Cl_{0.12}(OH)_{1.64}O_{2.51}Al_{0.02}(H_2O)_{0.95} + 0.29\ AlF_3{\cdot}3H_2O + 0.04\ Ti_3AlC_2$] HF-MXene. The $\Delta H_{ox,\ 700°C,\ total}$ was then corrected by removing the enthalpic contribution of the unreacted Ti_3AlC_2 MAX phase, $\Delta H_{ox,\ 700°C,\ MAX} = -1387.7 \pm 21.4$ kJ/mol Ti_3AlC_2 using the thermochemical cycle in **Table S2**. The remaining enthalpic effect is the enthalpy of drop oxidation calorimetry of MXene and $AlF_3{\cdot}3H_2O$ ($\Delta H_{ox,700°C,\ MXene+AlF3{\cdot}3H2O}$). The reaction describing the heating and oxidation of MXene and $AlF_3{\cdot}3H_2O$ is shown in **Equation 1**.

Equation 1:

$$Ti_3C_2F_\beta Cl_\gamma(OH)_\delta O_\varepsilon Al_\zeta Co_\eta(H_2O)_\kappa\ (25\ °C, s) + \mu\ AlF_3{\cdot}3H_2O\ (25\ °C, s) + [3 + 2 + 1.5(0.5\zeta+0.5\mu) + 2(0.33\eta) - 0.5(\delta+\varepsilon)]\ O_2\ (700\ °C, g) \rightarrow$$

$$3\ TiO_2\ (700\ °C, s) + 2\ CO_2\ (700\ °C, g) + (0.5\beta+1.5\mu)\ F_2\ (700\ °C, g) + 0.5\gamma\ Cl_2\ (700\ °C, g) + (0.5\zeta+0.5\mu)\ Al_2O_3\ (700\ °C, s) + 0.33\eta\ Co_3O_4\ (700\ °C, s) + (0.5\delta+\kappa+3\mu)\ H_2O\ (700\ °C, g)$$

$\Delta H_{ox,\ 700°C,\ MXene+AlF3{\cdot}3H2O} = -2254.0 \pm 35.3$ kJ/mol Ti_3C_2 (CoF_2-MXene), -2223.6 ± 35.1 kJ/mol Ti_3C_2 (HF-MXene)

At 700 °C, in atmospheric pressure, the Co^{2+} species is fully oxidized to Co_3O_4. [70] Using the thermochemical cycle in **Table S3**, the enthalpy of oxidation of MXene and $AlF_3{\cdot}3H_2O$ at 25 °C ($\Delta H_{ox,\ 25°C,\ MXene+AlF3{\cdot}3H2O}$) is derived. The reaction of the oxidation of MXene and $AlF_3{\cdot}3H_2O$ at 25 °C is presented in **Equation 2**.

Equation 2:

$$Ti_3C_2F_\beta Cl_\gamma(OH)_\delta O_\varepsilon Al_\zeta Co_\eta(H_2O)_\kappa\ (25\ °C, s) + \mu\ AlF_3{\cdot}3H_2O\ (25\ °C, s) + [3 + 2 + 1.5(0.5\zeta+0.5\mu) + 2(0.33\eta) - 0.5(\delta+\varepsilon)]\ O_2\ (25\ °C, g) \rightarrow$$

$$3\ TiO_2\ (25\ °C, s) + 2\ CO_2\ (25\ °C, g) + (0.5\beta+1.5\mu)\ F_2\ (25\ °C, g) + 0.5\gamma\ Cl_2\ (25\ °C, g)$$

+ (0.5ζ+0.5μ) Al_2O_3 (25 °C, s) + 0.33η Co_3O_4 (25 °C, s) + (0.5δ+κ+3μ) H_2O (25 °C, l)

$\Delta H_{ox,\ 25°C,\ MXene+AlF3\cdot3H2O}$ = – 2541.9 ± 35.3 kJ/mol Ti_3C_2 (CoF_2-MXene), – 2576.9 ± 35.1 kJ/mol Ti_3C_2 (HF-MXene)

Enthalpies of crystallization of $AlF_3 \cdot 3H_2O$ from AlF_3 and H_2O and enthalpies of oxidation of AlF_3 at 25 °C are calculated in **Table S4**. [71,72] These heat effects are used to derive the enthalpy of oxidation of $AlF_3 \cdot 3H_2O$ at 25 °C ($\Delta H_{ox,\ 25°C,\ AlF3\cdot3H2O}$ = – 1479.7 ± 10.2 kJ/mol $AlF_3 \cdot 3H_2O$) using the thermochemical cycle in **Table S5**. The enthalpy of oxidation of MXene at 25 °C ($\Delta H_{ox,\ 25°C,\ MXene}$) was derived by removing the enthalpic contribution of $\Delta H_{ox,\ 25°C,\ AlF3\cdot3H2O}$ from $\Delta H_{ox,\ 25°C,\ MXene+AlF3\cdot3H2O}$ using the thermochemical cycle presented in **Table S6**. The reaction of the oxidation of MXene at 25 °C is shown in **Equation 3**.

Equation 3:

$Ti_3C_2F_\beta Cl_\gamma(OH)_\delta O_\varepsilon Al_\zeta Co_\eta(H_2O)_\kappa$ (25 °C, s) + [3 + 2 + 1.5(0.5ζ) + 2(0.33η) – 0.5(δ + ε)] O_2 (25 °C, g) →

3 TiO_2 (25 °C, *s*) + 2 CO_2 (25 °C, g) + 0.5β F_2 (25 °C, g) + 0.5γ Cl_2 (25 °C, g) + 0.5ζ Al_2O_3 (25 °C, s)

+ 0.33η Co_3O_4 (25 °C, s) + (0.5δ+ κ) H_2O (25 °C, l)

$\Delta H_{ox,25°C,\ MXene}$ = – 2320.0 ± 35.5 kJ/mol Ti_3C_2 (CoF_2-MXene), – 2147.7 ± 35.5 kJ/mol Ti_3C_2 (HF-MXene)

Subsequently, to calculate the enthalpy of formation from elements of MXene at 25 °C ($\Delta H_{f,\ 25°C,\ MXene}$), we use the thermochemical cycle in **Table S7**. The reaction of the formation of MXene from elements at 25 °C is presented in **Equation 4**.

Equation 4:

3 Ti (25 °C, *s*) + 2 C (25 °C, g) + 0.5β F_2 (25 °C, g) + 0.5γ Cl_2 (25 °C, g) + ζ Al (25 °C, s) + η Co (25 °C, s)

+ (0.5δ+ κ) H_2 + (0.5δ + 0.5ε + κ)] O_2 (25 °C, g) →

$Ti_3C_2F_\beta Cl_\gamma(OH)_\delta O_\varepsilon Al_\zeta Co_\eta(H_2O)_\kappa$ (25 °C, s)

$\Delta H_{f,\ 25°C,\ MXene}$ = – 1891.7 ± 35.7 kJ/mol Ti_3C_2 (CoF_2-MXene), – 1978.2 ± 35.7 kJ/mol Ti_3C_2 (HF-MXene)

The thermochemical results are summarized and compared with experimentally derived literature values for a $Ti_3C_2T_x$ MXene etched in a LiF/HCl environment (LiF-MXene, see **Table 3**). The

etching process of LiF-MXene is described in detail by *Ghidiu et al*.[10] This etching route is known to intercalate Li^+ ions during synthesis and produce large interlayer spacings (27 – 28 Å). Compared with our etching approach, this is quite similar. Both etching methods have the same pH, with relatively high amounts of F^- ions. [15] It was also assumed that their pre-treatment conditions removed all interlayer water, so water was not included in the compositions of their MXenes. However, in another report on the same set of samples, it was speculated that there appeared to be intercalated water filling the interlayer spaces that were, in fact, not removed. [41]

Table 3. Compositions, enthalpies of oxidation, and enthalpies of formation from elements of MXenes.

Sample	Composition	$\Delta H_{ox,25°C}$ (kJ/mol Ti_3C_2)	$\Delta H_{f,25°C}$ (kJ/mol Ti_3C_2)
CoF_2-MXene	$Ti_3C_2F_{1.05}Cl_{0.09}(OH)_{1.15}O_{3.10}Al_{0.26}Co_{0.03}(H_2O)_{0.76}$	-2320.0 ± 35.5	-1891.7 ± 35.7
HF-MXene	$Ti_3C_2F_{1.71}Cl_{0.12}(OH)_{1.64}O_{2.51}Al_{0.02}(H_2O)_{0.95}$	-2147.7 ± 35.5	-1978.2 ± 35.1
LiF-MXene	$Ti_3C_2F_{0.25}Cl_{0.02}(OH)_{0.06}O_{0.84}Li_{0.38}$	-1917.0 ± 3.7 [28]	-1908.2 ± 5.4 [28]

The formation enthalpy of the LiF-MXene sample is derived from high-temperature oxide melt drop solution calorimetry retrieved from *Sharma et al.* [28] The LiF-MXene sample is synthesized with LiF/HCl as the etching agent as described by *Ghidiu et al.* [10] Values are in kJ/mol Ti_3C_2 were MXene is defined as the composition stated.

The enthalpies of formation of CoF_2-MXene and HF-MXene from this study and LiF-MXene and Ti_3AlC_2 MAX reported by *Sharma et al.* are presented in **Figure 5a**. [28] The $\Delta H_{f,\,25°C,\,MXene}$ for all three MXenes synthesized with different etching agents (CoF_2/HCl, HF/HCl, and LiF/HCl) are strongly exothermic with around 100 kJ/mol Ti_3C_2 difference among each other. All

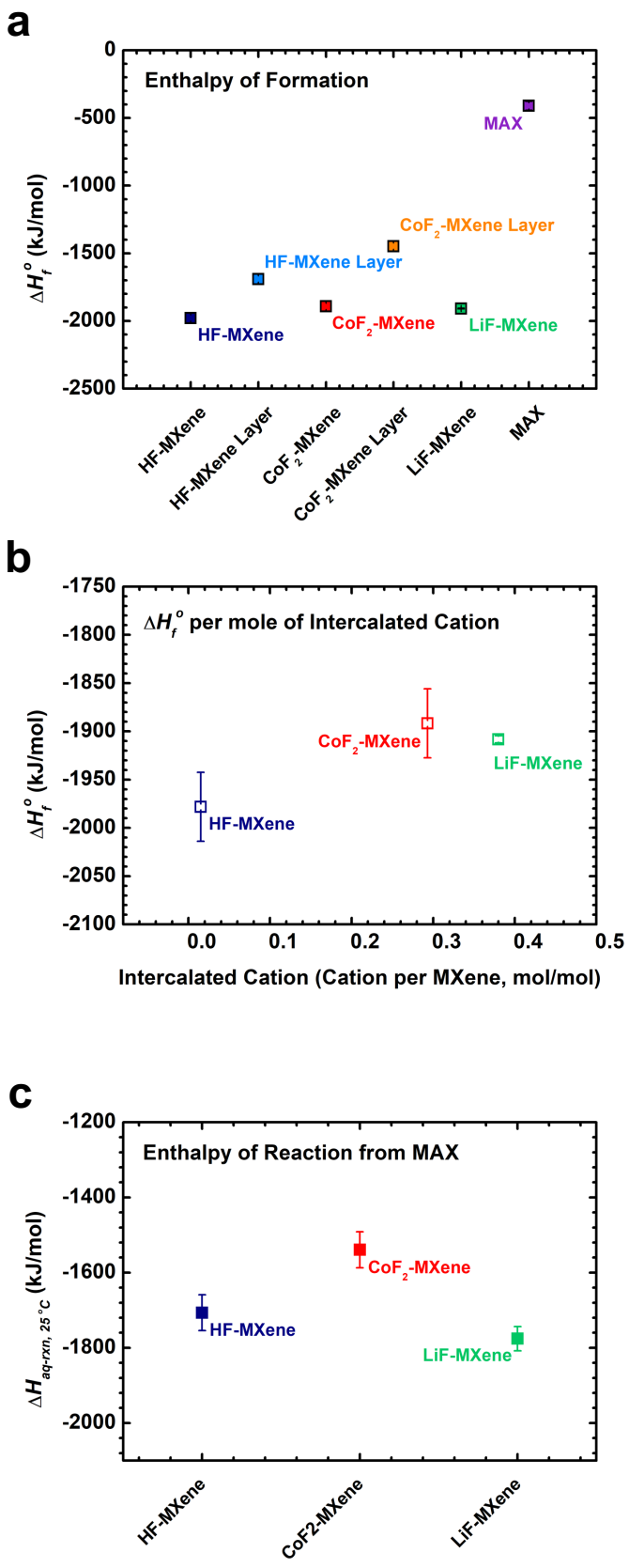

Figure 5. (**a**) Enthalpies of formation from elements of MXenes and MAX, (**b**) enthalpies of formation of MXenes as a function of the content of intercalated cations, and (**c**) enthalpy of reaction from MAX to MXenes in solution at 25 °C. The formation enthalpy data of LiF-MXene and MAX (Ti_3AlC_2) is retrieved from Sharma et al. and derived from high-temperature oxide melt drop solution calorimetry. [28] LiF-MXene is $Ti_3C_2T_x$ MXene synthesized in LiF/HCl as described by Ghidiu et al. [10]

MXenes are significantly more exothermic than the enthalpy of formation from elements of the Ti_3AlC_2 MAX phase, – 409.8 ± 31.9 kJ/mol Ti_3AlC_2. [28] HF-MXene presents the most exothermic formation enthalpy. Specifically, the $\Delta H_{f,25^\circ C}$ of HF-MXene is ~ 86.5 kJ/mol Ti_3C_2 more exothermic than CoF_2-MXene, and ~ 70 kJ/mol Ti_3C_2 more exothermic than that of LiF-MXene.

Manipulation of MXene Energetics by Intercalated Cationic Species

The major compositional and structural differences between CoF_2-MXene and HF-MXene are in the (*i*) content of cations and the (*ii*) degree of hydration within the interlayer space. To elucidate the formation enthalpy from elements of MXene's dependence on cationic content, we plot the enthalpy of formation from elements as a function of cationic content per Ti_3C_2 unit in **Figure 5b**. CoF_2-MXene contains Al^{3+} and Co^{2+} as the interlayer cations, which results in larger interlayer spacings and interlayer heterogeneity. Using density functional theory (DFT), *Berdiyorov and Mahmoud* calculated the differences in total energy of the system due to insertion of ions into MXenes with different termination groups, including $Ti_3C_2F_2$ and $Ti_3C_2O_2$. The system is defined as $Ti_3C_2T_x$, where T_x is either O_2 or F_2. They predicted the energy change from insertion of Al^{3+} is 320 kJ/mol Ti_3C_2 (~3.3 eV/atom) less exothermic for $Ti_3C_2F_2$ and 250 kJ/mol Ti_3C_2 (~2.6 eV/atom) less exothermic for $Ti_3C_2O_2$. [73] Less exothermic formation enthalpies from elements were generated from the increase in interlayer spacing that the cation insertion caused. [73] Applying these predicted energy changes, if the 0.24 additional Al^{3+} that CoF_2-MXene holds is inserted into HF-MXene, the enthalpy of formation from elements for HF-MXene would become ~ 60 to 83 kJ/mol Ti_3C_2 less exothermic, close to the 86.5 kJ/mol Ti_3C_2 calculated difference we found. Although, HF-MXene appears to be significantly different compared to LiF-MXene, especially considering its surface chemistry. Here, we perform the same interpretation on this set

of thermodynamic data. It is also predicted that the insertion of Li^+ ions changes the energy 150 kJ/mol Ti_3C_2 (~1.5 eV/atom) less exothermic for both $Ti_3C_2F_2$ and $Ti_3C_2O_2$. [73] Similarly, using the Li composition of LiF-MXene, an energy change of ~57 kJ/mol Ti_3C_2 less exothermic would result upon the 0.38 mol Li inserted into a non-intercalated Ti_3C_2 MXene, close to the 70 kJ/mol Ti_3C_2 energetic difference between LiF-MXene and HF-MXene. Thus, it is highly likely that the less exothermic formation enthalpy from elements of CoF_2-MXene is closely related to the expanded interlayer distances caused by the intercalation of Co^{2+} and Al^{3+} within the interlayer space. Indeed, it is a common phenomenon that cationic intercalation increases the interlayer distances of MXenes, leading to reduced layer–layer van der Waals forces. [35,37,73] Because of the larger distribution of the interlayer distances of CoF_2-MXene, particularly the increased interlayer distance due to pillaring, the layer–layer van der Waals forces are not as strong. Consequently, the carbide layers of CoF_2-MXene tend not to stabilize each other as much as those layers of HF-MXene that are uniformly apart and with smaller interlayer distances.

Degree and Energetics of Interlayer Hydration

The high degree of hydration of HF-MXene also effectively stabilizes the surface defects and functional groups through hydrogen bonding. Synthesized under aqueous acidic environments, $Ti_3C_2T_x$ MXene has well-known hydrophilicity. [10,74–77] The replacement of -F surface groups by -OH and -O leads to spontaneous water intercalation due to their higher hydrophilicity. [78] Furthermore, upon heating, the $Ti_3C_2T_x$ MXenes with more -F groups release water at lower temperatures than those with less -F. [79] According to calorimetric results, the $Ti_3C_2T_x$ MXenes' surface is weakly hydrophilic, exhibiting a low magnitude of water adsorption enthalpies and weakly exothermic enthalpies of immersion in water. [41] Based on our interpretation, higher surface oxygen -O concentration results in more potent hydration effects. Water has strongly exothermic

interactions with TiO_2 nanoparticles. [80] Similarly, it was predicted that the energetic impact of hydration of the $Ti_3C_2O_2$ layer was increasingly exothermic as the degree of hydration increased from 0 to 1 mole H_2O per mole of $Ti_3C_2O_2$. [81] Exacerbating the lack of hydration effects in CoF_2-MXene, interlayer Al^{3+} is expected to be adsorbed onto the -O surface groups. [60] Thus, we conclude that the formation enthalpies from elements of CoF_2-MXene and HF-MXene are modified by the intercalated cationic species, decreased layer-layer van der Waals forces, and the degree and energetics of hydration. Hydration may play a more significant role in contributing to the exothermic enthalpy of formation from elements of MXenes than van der Waals forces. Hydrogen bonding is generally assigned interaction strengths of 4 – 40 kJ/mol per atom pair, an order of magnitude greater than van der Waals forces, 0.4 – 4 kJ/mol per atom pair. [82,83]

Entropic Contributions of Interlayer Cations

Furthermore, the metal ions confined within the interlayer space may have significant entropic effects on the intercalated water, directing the local order of interlayer-confined water. Using inelastic neutron scattering techniques and molecular dynamics (MD) simulation, the interlayer water in HF etched $Ti_3C_2T_x$ MXene was "bulklike" in character with the significant disorder. [61] However, as the intercalated metal ions are introduced, the confinement effects lead to water molecules with a greater interlayer order. [61] Among cation-intercalated $Ti_3C_2T_x$ MXenes, this relationship appears not to be a function of interlayer distance, as the interlayer distances are near-identical. [61] The highly ordered water on the surface of TiO_2 nanoparticles led to a decrease in entropy compared to ice for both anatase and rutile phases. [84,85] In another study, it was found that in MD simulations, Al^{3+} features two distinct hydration shells while intercalated. [86] Therefore, in this study, we anticipate that the water confined in CoF_2-MXene is higher in order or has lower entropy compared with that intercalated within the interlayer space of HF-MXene.

Intralayer Termination Groups

To distinguish the effect of the intralayer on the formation enthalpies from elements, we separate the exothermic contributions of Al_2O_3, Co_3O_4, and adsorbed H_2O from the enthalpy of formation from elements. We estimate this to be the energetic effects of MXene intralayer formation ($\boldsymbol{\Delta H_{f,25°C,\ MXene\text{-}layer}}$) and calculate this using the thermochemical cycle presented in **Table S8**. The reaction of the formation of MXene from elements and Al_2O_3, Co_3O_4, and "free" H_2O at 25 °C is presented in **Equation 5**.

Equation 5:

$$3\ Ti\ (25\ °C,\ s) + 2\ C\ (25\ °C,\ g) + 0.5\beta\ F_2\ (25\ °C,\ g) + 0.5\gamma\ Cl_2\ (25\ °C,\ g)\ 0.5\delta\ H_2$$

$$+ (0.5\delta + 0.5\varepsilon - 0.75\zeta - 0.66\ \eta - 0.5\kappa)\ O_2\ (25\ °C,\ g) + 0.5\zeta\ Al_2O_3\ (25\ °C,\ s) + 0.33\eta\ Co_3O_4\ (25\ °C,\ s)$$

$$+ \kappa\ H_2O\ (25\ °C,\ l) \rightarrow$$

$$Ti_3C_2F_\beta Cl_\gamma(OH)_\delta O_\varepsilon Al_\zeta Co_\eta(H_2O)_\kappa\ (25\ °C,\ s)$$

$\boldsymbol{\Delta H_{f,25°C,MXene\text{-}layer}}$ = – 1447.6 ± 35.7 kJ/mol Ti_3C_2 (CoF_2-MXene), – 1689.9 ± 35.7 kJ/mol Ti_3C_2 (HF-MXene)

Markedly, even with the contributions from the interlayer water and intercalated cationic species subtracted, both CoF_2-MXene and HF-MXene present strongly exothermic enthalpies of formation from elements (see **Figure 5a**). Earlier several studies have predicted enthalpies of formation from elements for Ti_3C_2 MXene without surface functionalization or termination groups to have – 176.15 kJ/mol Ti_3C_2 (– 0.365 eV/atom) [87] and – 115 kJ/mol Ti_3C_2 (– 0.238 eV/atom) using the first-principle calculations. [88] These predictions lead to models with significantly less exothermic enthalpies of formation from elements compared to $Ti_3C_2T_x$ MXenes with termination groups. The significant differences in formation enthalpies from elements between our experimentally measured thermodynamic data and these predicted values highlight the crucial roles of surface terminations in the effective stabilization of $Ti_3C_2T_x$ MXenes. In addition, using a multiscale computational approach, it was found that surface functionalization had a strong, energetic driving

force and was primarily dependent on external conditions and not the intralayer composition of MXene. [31] The enthalpies of formation from elements have been calculated using first principle methods to be – 1233, – 1843, and – 1191 kJ/mol Ti_3C_2 for ideal $Ti_3C_2O_2$, $Ti_3C_2F_2$, and $Ti_3C_2(OH)_2$, respectively, suggesting that these modeled materials with termination groups are energetically favorable. [29] We use these computational data to interpret the enthalpies of formation from elements for $Ti_3C_2T_x$ MXenes with the same ratio of functional groups at ideal stoichiometry, x = 2.0. We estimate these values using simple mechanical mixing, which does not incorporate any interactivity among functional groups (see **Equation 6**).

Equation 6:

$$\Delta H_{f,ideal\text{-}mix} = \varepsilon\, \Delta H_{f,ideal,Ti3C2O2} + \beta\, \Delta H_{f,ideal,Ti3C2F2} + \delta\, \Delta H_{f,ideal,Ti3C2OH2}$$

where $O_\varepsilon F_\beta OH_\delta$, CoF_2-MXene ratio is $O_{0.58}F_{0.19}OH_{0.21}Cl_{0.02}$ and HF-MXene ratio is $O_{0.42}F_{0.29}OH_{0.27}Cl_{0.02}$.

Our model samples' estimated $\Delta H_{f,ideal\text{-}mix}$ values are – 1315 kJ/mol Ti_3C_2 with a CoF_2-MXene balance and – 1374 kJ/mol Ti_3C_2 with an HF-MXene balance. The presence of Cl^- is neglected because of its low content. A comparison of CoF_2-MXene and HF-MXene with these modeled "hypothetical" structures suggests that $\Delta H_{f,ideal\text{-}mix}$ from elements of these ideal systems are significantly less exothermic than either of the enthalpies of formation from elements and compounds we derive, $\Delta H_{f,25°C,\,MXene}$ or $\Delta H_{f,25°C,\,MXene\text{-}layer}$. In other words, our experimental results reflect that the surface functionalization enables more exothermic formation enthalpies from elements along with that of intercalated species.

To investigate the thermodynamic driving forces present in a model etching environment, we further calculated the enthalpy of reaction from Ti_3AlC_2 MAX to $Ti_3C_2T_x$ MXenes in solution at 25 °C ($\Delta H_{aq\text{-}rxn,25°C}$) from $\Delta H_{f,25°C,\,MXene}$ of CoF_2-MXene and HF-MXene using the thermochemical cycle in **Table S9**. Considering the significantly favorable exothermic etching reaction and low surface area of bulk MAX ceramics, the energetic effects of MAX hydration are

neglected. The reaction of the formation from elements of MXene from MAX through etching in solution at 25 °C is presented in **Equation 7** (see **Figure 5c**).

Equation 7:

$$Ti_3AlC_2\ (25\ °C, s) + \beta\ F^-\ (25\ °C, aq) + \gamma\ Cl^-\ (25\ °C, aq) + \eta\ Co^{2+}\ (25\ °C, aq) + \delta\ H^+\ (25\ °C, aq)$$

$$+ (0.5\delta + 0.5\varepsilon)\ O_2\ (25\ °C, g) + 3\mu\ H_2O\ (25\ °C, l) + \kappa\ H_2O\ (25\ °C, ad) \rightarrow$$

$$(1 - \alpha)\ Ti_3C_2F_\beta Cl_\gamma(OH)_\delta O_\varepsilon Al_\zeta Co_\eta(H_2O)_\kappa\ (25\ °C, s) + \alpha\ Ti_3AlC_2 + \mu\ AlF_3{\cdot}3H_2O\ (25\ °C, s)$$

$$+ (1 - \alpha - \mu - \zeta)\ Al^{3+}\ (25\ °C, aq)$$

$$\Delta H_{aq\text{-}rxn,25°C} = -1539.3 \pm 47.7\ \text{kJ/mol}\ Ti_3C_2\ (CoF_2\text{-MXene}),\ -1706.5 \pm 47.8\ \text{kJ/mol}\ Ti_3C_2\ (\text{HF-MXene})$$

The $\Delta H_{aq\text{-}rxn,25°C}$ of Ti_3AlC_2 MAX to CoF_2-MXene (– 1539.3± 47.7 kJ/mol Ti_3C_2) is less exothermic than that of Ti_3AlC_2 MAX to HF-MXene (– 1706.5 ± 47.8 kJ/mol Ti_3C_2), both of which are strongly exothermic. This interpretation suggests a clear driving force for the etching process from Ti_3AlC_2 MAX to the formation of $Ti_3C_2T_x$ MXenes. Our findings align with the thermodynamic study on LiF-MXene by *Sharma et al.*, with $\Delta H_{aq\text{-}rxn,25°C}$ of – 1775.6 ± 32.2 kJ/mol Ti_3C_2. [28] Hence, the analysis above highlights the strong thermodynamic driving force of the etching environments for the formation of $Ti_3C_2T_x$ MXene from Ti_3AlC_2 MAX even at room temperature. [15]

The research performed here enables fundamental knowledge of the effects of layer–layer affinity and the effects of intercalants on the formation enthalpies of MXenes from elements synthesized under different etching conditions. These insights are crucial, as precise manipulation of the interlayer space is the go-to engineering tool used to control the properties and performances of MXenes and two-dimensional materials in general. As part of our ongoing studies on MXenes, advanced experimental studies on the refined local structure and orientation of species intercalated within the MXene layers with a systematically varied interlayer distance using a variety of intercalants will further enhance our understanding of the synthesis, interfacial chemistry, and their

relations with the properties of MXenes. Furthermore, the complexity and heterogeneity of the system and composition of MXenes are often intentionally neglected to simplify experimental results and computational predictions, frequently assuming layer to layer homogeneity and stoichiometric surface chemistry. Commonly, impurities such as TiO_2 and $AlF_3{\cdot}3H_2O$ and unreacted Ti_3AlC_2 are ignored because they are difficult to quantify. Despite MXene's inherent complexities, from a thermodynamic perspective, we provide vision into the intercalates – layer and layer – layer interfacial interactions of as-synthesized MXenes by integrating our calorimetric studies with models from computational predictions and experimental observations from the literature.

Conclusions

We etched $Ti_3C_2T_x$ MXenes in two different environments leading to similar layer chemistries but different structures and intercalant compositions. By investigating these MXene's thermochemistry using high-temperature oxidation drop calorimetry, we correlate the derived thermodynamic stabilities with compositional, structural, and interfacial properties caused by the variation of etching environments. We derive the enthalpies of formation from elements at 25 °C. The surface functionalization of the MXene layers significantly impacts their formation enthalpy from elements. Specifically, CoF_2-MXene and HF-MXene exhibit beyond stoichiometric surface functionalization leading to more exothermic enthalpies of formation from elements than computationally derived ideal $Ti_3C_2T_x$ MXenes, even when the exothermic contributions of interlayer species are removed. Interestingly, we find that CoF_2-MXene has an exothermic enthalpy of formation from elements than HF-MXene. The more exothermic enthalpy of formation of HF-MXene primarily originates from two factors: (*i*) HF-MXene features a higher degree of hydration, filling the interlayer spaces and leading to more effective stabilization of the layer-

possessed functional groups; and (*ii*) HF-MXene has a lower and more uniform dimension of interlayer space, which results in stronger van der Waals forces between the adjacent planar surfaces, in other words, stronger layer–layer interactions. CoF_2-MXene has more interlayer cationic contents, Al^{3+} and Co^{2+}, largely Al^{3+}. These intercalated cationic species displace the interlayer water and competitively bind to the surface functional groups of MXenes. Additionally, the cations act as pillaring agents, expanding the layer to layer distance of CoF_2-MXene in some of the interlayer spaces, resulting in a broader distribution of interlayer distances with higher average d-spacings. Both samples have a significantly larger exothermic enthalpy of formation from elements than the Ti_3AlC_2 MAX parent phase. Moreover, we demonstrate that in an aqueous medium, the derived enthalpies of reaction from Ti_3AlC_2 MAX to $Ti_3C_2T_x$ MXenes are exothermic, reflecting the driving force of etching in synthesis conditions. This study provides new insights into the energetic–structure–surface property relationships of MXenes and highlights the complexities of guest–host interactions in MXenes involving water, cations, and a spectrum of surface functional groups. The fundamental thermochemical insights on $Ti_3C_2T_x$ MXenes etched with CoF_2/HCl aqueous solution gained here may aid the design and modification of MXene materials for precisely tuned compositional, interfacial, and nanostructural properties.

Acknowledgments

Di Wu acknowledges the fund of Alexandra Navrotsky Institute for Experimental Thermodynamics and the institutional funds from the Gene and Linda Voiland School of Chemical Engineering and Bioengineering at Washington State University. Los Alamos National Laboratory, an affirmative action-equal opportunity employer, is managed by Triad National Security, LLC for the U.S. Department of Energy's NNSA, under contract 89233218CNA000001.

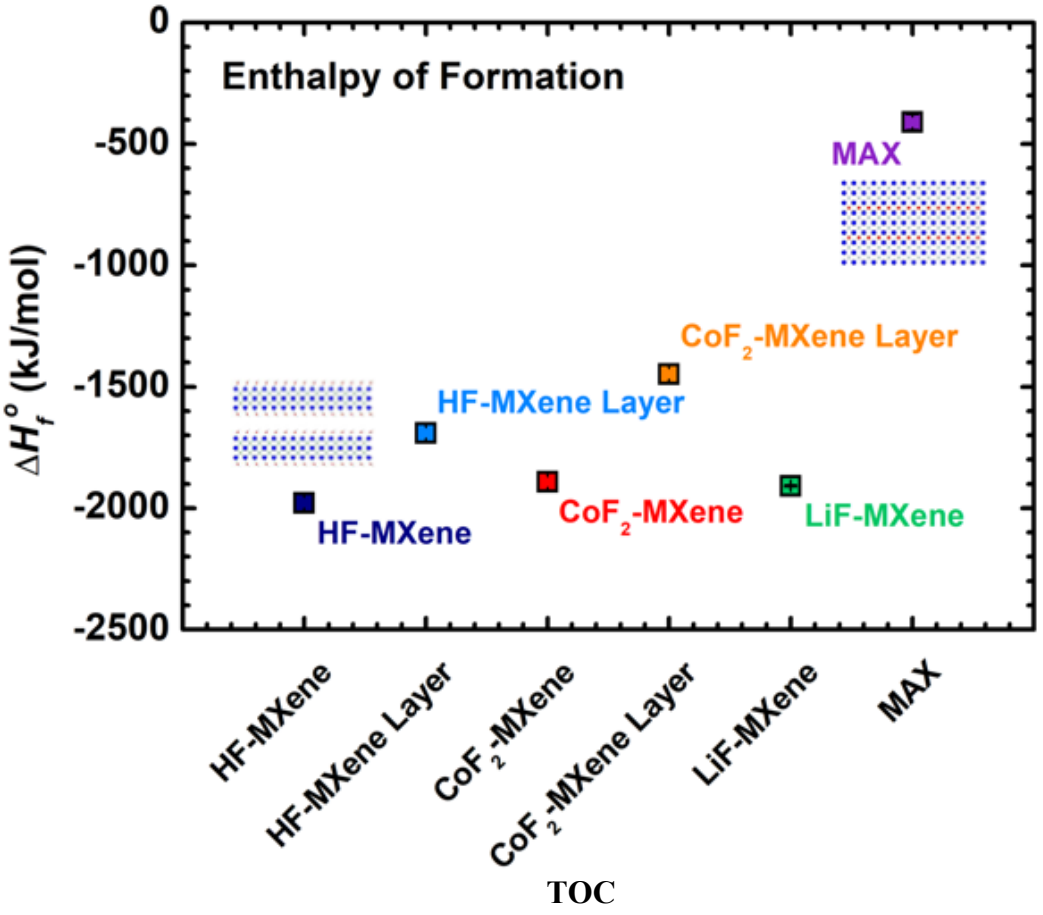
Enthalpy of Formation
ΔH_f° (kJ/mol)
0
-500
-1000
-1500
-2000
-2500
MAX
CoF_2-MXene Layer
HF-MXene Layer
HF-MXene
CoF_2-MXene
LiF-MXene
HF-MXene
HF-MXene Layer
CoF_2-MXene
CoF_2-MXene Layer
LiF-MXene
MAX

TOC

References

(1) Anasori, B.; Lukatskaya, M. R.; Gogotsi, Y. 2D Metal Carbides and Nitrides (MXenes) for Energy Storage. *Nat. Rev. Mater.* **2017**, *2*, 16098. https://doi.org/10.1038/natrevmats.2016.98.

(2) Sohan, A.; Banoth, P.; Aleksandrova, M.; Nirmala Grace, A.; Kollu, P. Review on MXene Synthesis, Properties, and Recent Research Exploring Electrode Architecture for Supercapacitor Applications. *Int. J. Energy Res.* **2021**, *45* (14), 19746–19771. https://doi.org/10.1002/er.7068.

(3) Murali, G.; Rawal, J.; Modigunta, J. K. R.; Park, Y. H.; Lee, J.-H.; Lee, S.-Y.; Park, S.-J.; In, I. A Review on MXenes: New-Generation 2D Materials for Supercapacitors. *Sustain. Energy Fuels* **2021**, *5* (22), 5672–5693. https://doi.org/10.1039/D1SE00918D.

(4) Li, X.; Wan, G.; Xiao, J.; Wu, L.; Shi, S.; Wang, G. Carbon-Coated Ni(OH)2-NiAl LDH Hierarchical Nanostructures on Ni Foam as a High Areal Capacitance Electrode for Supercapacitor Application. *Mater. Lett.* **2018**, *228*, 179–182. https://doi.org/10.1016/j.matlet.2018.06.012.

(5) Lukatskaya, M. R.; Kota, S.; Lin, Z.; Zhao, M.-Q.; Shpigel, N.; Levi, M. D.; Halim, J.; Taberna, P.-L.; Barsoum, M. W.; Simon, P.; Gogotsi, Y. Ultra-High-Rate Pseudocapacitive Energy Storage in Two-Dimensional Transition Metal Carbides. *Nat. Energy* **2017**, *2* (8), 17105. https://doi.org/10.1038/nenergy.2017.105.

(6) Chaudhari, N. K.; Jin, H.; Kim, B.; San Baek, D.; Joo, S. H.; Lee, K. MXene: An Emerging Two-Dimensional Material for Future Energy Conversion and Storage Applications. *J. Mater. Chem. A* **2017**, *5* (47), 24564–24579. https://doi.org/10.1039/c7ta09094c.

(7) Gogotsi, Y.; Anasori, B. The Rise of MXenes. *ACS Nano* **2019**, *13* (8), 8491–8494. https://doi.org/10.1021/acsnano.9b06394.

(8) Xu, J.; Peng, T.; Qin, X.; Zhang, Q.; Liu, T.; Dai, W.; Chen, B.; Yu, H.; Shi, S. Recent Advances in 2D MXenes: Preparation, Intercalation and Applications in Flexible Devices. *J. Mater. Chem. A* **2021**, *9* (25), 14147–14171. https://doi.org/10.1039/D1TA03070A.

(9) Voigt, C. A.; Ghidiu, M.; Natu, V.; Barsoum, M. W. Anion Adsorption, Ti3C2Tz MXene Multilayers, and Their Effect on Claylike Swelling. *J. Phys. Chem. C* **2018**, *122* (40), 23172–23179. https://doi.org/10.1021/acs.jpcc.8b07447.

(10) Ghidiu, M.; Lukatskaya, M. R.; Zhao, M. Q.; Gogotsi, Y.; Barsoum, M. W. Conductive Two-Dimensional Titanium Carbide "clay" with High Volumetric Capacitance. *Nature* **2015**, *516* (7529), 78–81. https://doi.org/10.1038/nature13970.

(11) Wahid, Z.; A., M. R.; W., T. M.; Yu-Hsuan, L.; Yousuf, B.; B., D. M.; Slavomir, N.; Ethan, C.; C., H. M.; T., C. P.; B., H. K. In Situ Investigation of Water on MXene Interfaces. *Proc. Natl. Acad. Sci.* **2021**, *118* (49), e2108325118. https://doi.org/10.1073/pnas.2108325118.

(12) Luo, J.; Zhang, W.; Yuan, H.; Jin, C.; Zhang, L.; Huang, H.; Liang, C.; Xia, Y.; Zhang, J.; Gan, Y.; Tao, X. Pillared Structure Design of MXene with Ultralarge Interlayer Spacing for High-Performance Lithium-Ion Capacitors. *ACS Nano* **2017**, *11* (3), 2459–2469.

https://doi.org/10.1021/acsnano.6b07668.

(13) Ghidiu, M.; Halim, J.; Kota, S.; Bish, D.; Gogotsi, Y.; Barsoum, M. W. Ion-Exchange and Cation Solvation Reactions in Ti3C2 MXene. *Chem. Mater.* **2016**, *28* (10), 3507–3514. https://doi.org/10.1021/acs.chemmater.6b01275.

(14) Naguib, M.; Kurtoglu, M.; Presser, V.; Lu, J.; Niu, J.; Heon, M.; Hultman, L.; Gogotsi, Y.; Barsoum, M. W. Two-Dimensional Nanocrystals Produced by Exfoliation of Ti3AlC2. *Adv. Mater.* **2011**, *23* (37), 4248–4253. https://doi.org/10.1002/adma.201102306.

(15) Alhabeb, M.; Maleski, K.; Anasori, B.; Lelyukh, P.; Clark, L.; Sin, S.; Gogotsi, Y.; Alhabeb, M.; Clark, L.; Anasori, B.; Sin, S.; Maleski, K.; Lelyukh, P. Guidelines for Synthesis and Processing of Two-Dimensional Titanium Carbide (Ti3C2Tx MXene). *Chem. Mater.* **2017**, *29* (18), 7633–7644. https://doi.org/10.1021/acs.chemmater.7b02847.

(16) Chen, J.; Jia, J.; Zhou, A.; Hu, Q.; Zhou, W.; Liu, F.; Wang, L. Preparation of Ti 3 C 2 and Ti 2 C MXenes by Fluoride Salts Etching and Methane Adsorptive Properties. *Appl. Surf. Sci.* **2017**, *416*, 781–789. https://doi.org/10.1016/j.apsusc.2017.04.239.

(17) Wang, X.; Garnero, C.; Rochard, G.; Magne, D.; Morisset, S.; Hurand, S.; Chartier, P.; Rousseau, J.; Cabioc'H, T.; Coutanceau, C.; Mauchamp, V.; Célérier, S. A New Etching Environment (FeF3/HCl) for the Synthesis of Two-Dimensional Titanium Carbide MXenes: A Route towards Selective Reactivity: Vs. Water. *J. Mater. Chem. A* **2017**, *5* (41), 22012–22023. https://doi.org/10.1039/c7ta01082f.

(18) Cockreham, C.; Zhang, X.; Li, H.; Hammond-Pereira, E.; Sun, J.; Saunders, S. R.; Wang, Y.; Xu, H.; Wu, D. Inhibition of AlF3·3H2O Impurity Formation in Ti3C2Tx MXene Synthesis under a Unique CoFx/HCl Etching Environment. *ACS Appl. Energy Mater.* **2019**. https://doi.org/10.1021/acsaem.9b01618.

(19) Benchakar, M.; Loupias, L.; Garnero, C.; Bilyk, T.; Morais, C.; Canaff, C.; Guignard, N.; Morisset, S.; Pazniak, H.; Hurand, S.; Chartier, P.; Pacaud, J.; Mauchamp, V.; Barsoum, M. W.; Habrioux, A.; Célérier, S. One MAX Phase, Different MXenes: A Guideline to Understand the Crucial Role of Etching Conditions on Ti3C2Tx Surface Chemistry. *Appl. Surf. Sci.* **2020**, *530*, 147209. https://doi.org/10.1016/j.apsusc.2020.147209.

(20) Ronchi, R. M.; Arantes, J. T.; Santos, S. F. Synthesis, Structure, Properties and Applications of MXenes: Current Status and Perspectives. *Ceram. Int.* **2019**, *45* (15), 18167–18188. https://doi.org/10.1016/j.ceramint.2019.06.114.

(21) Xia, Y.; Mathis, T. S.; Zhao, M.-Q.; Anasori, B.; Dang, A.; Zhou, Z.; Cho, H.; Gogotsi, Y.; Yang, S. Thickness-Independent Capacitance of Vertically Aligned Liquid-Crystalline MXenes. *Nature* **2018**, *557* (7705), 409–412. https://doi.org/10.1038/s41586-018-0109-z.

(22) Shayesteh Zeraati, A.; Mirkhani, S. A.; Sun, P.; Naguib, M.; Braun, P. V; Sundararaj, U. Improved Synthesis of Ti3C2Tx MXenes Resulting in Exceptional Electrical Conductivity, High Synthesis Yield, and Enhanced Capacitance. *Nanoscale* **2021**, *13* (6), 3572–3580. https://doi.org/10.1039/D0NR06671K.

(23) Seredych, M.; Shuck, C. E.; Pinto, D.; Alhabeb, M.; Precetti, E.; Deysher, G.; Anasori, B.; Kurra, N.; Gogotsi, Y. High-Temperature Behavior and Surface Chemistry of Carbide

MXenes Studied by Thermal Analysis. *Chem. Mater.* **2019**, *31* (9), 3324–3332. https://doi.org/10.1021/acs.chemmater.9b00397.

(24) Mashtalir, O.; Naguib, M.; Mochalin, V. N.; Dall'Agnese, Y.; Heon, M.; Barsoum, M. W.; Gogotsi, Y. Intercalation and Delamination of Layered Carbides and Carbonitrides. *Nat. Commun.* **2013**, *4* (1), 1716. https://doi.org/10.1038/ncomms2664.

(25) Corbillon, M. S.; Olazabal, M. A.; Madariaga, J. M. Potentiometric Study of Aluminium-Fluoride Complexation Equilibria and Definition of the Thermodynamic Model. *J. Solution Chem.* **2008**, *37* (4), 567–579. https://doi.org/10.1007/s10953-008-9257-3.

(26) Rajavel, K.; Ke, T.; Yang, K.; Lin, D. Condition Optimization for Exfoliation of Two Dimensional Titanium Carbide (Ti3C2Tx). *Nanotechnology* **2018**, *29* (9), 95605. https://doi.org/10.1088/1361-6528/aaa687.

(27) Cockreham, C. B.; Zhang, X.; Eakin, J. A.; Dewa, M.; Li, H.; Li, N.; Sun, J.; Ha, S.; Ivory, C. F.; Wang, Y.; Xu, H.; Wu, D. Unveiling the Interfacial and Structural Heterogeneity of Ti3C2TxMXene Etched with CoF2/HCl by Integrated in Situ Thermal Analysis. *ACS Appl. Mater. Interfaces* **2021**, *13* (44), 52125–52133. https://doi.org/10.1021/acsami.1c10021.

(28) Sharma, G.; Naguib, M.; Feng, D.; Gogotsi, Y.; Navrotsky, A. Calorimetric Determination of Thermodynamic Stability of MAX and MXene Phases. *J. Phys. Chem. C* **2016**, *120* (49), 28131–28137. https://doi.org/10.1021/acs.jpcc.6b10241.

(29) Ashton, M.; Mathew, K.; Hennig, R. G.; Sinnott, S. B. Predicted Surface Composition and Thermodynamic Stability of MXenes in Solution. *J. Phys. Chem. C* **2016**, *120* (6), 3550–3556. https://doi.org/10.1021/acs.jpcc.5b11887.

(30) Björk, J.; Rosen, J. Functionalizing MXenes by Tailoring Surface Terminations in Different Chemical Environments. *Chem. Mater.* **2021**, *33* (23), 9108–9118. https://doi.org/10.1021/acs.chemmater.1c01264.

(31) Ibragimova, R.; Erhart, P.; Rinke, P.; Komsa, H.-P. Surface Functionalization of 2D MXenes: Trends in Distribution, Composition, and Electronic Properties. *J. Phys. Chem. Lett.* **2021**, *12* (9), 2377–2384. https://doi.org/10.1021/acs.jpclett.0c03710.

(32) Hu, T.; Hu, M.; Gao, B.; Li, W.; Wang, X. Screening Surface Structure of MXenes by High-Throughput Computation and Vibrational Spectroscopic Confirmation. *J. Phys. Chem. C* **2018**, *122* (32), 18501–18509. https://doi.org/10.1021/acs.jpcc.8b04427.

(33) Pandey, M.; Thygesen, K. S. Two-Dimensional MXenes as Catalysts for Electrochemical Hydrogen Evolution: A Computational Screening Study. *J. Phys. Chem. C* **2017**, *121* (25), 13593–13598. https://doi.org/10.1021/acs.jpcc.7b05270.

(34) Wahid, Z.; A., M. R.; W., T. M.; Yu-Hsuan, L.; Yousuf, B.; B., D. M.; Slavomir, N.; Ethan, C.; C., H. M.; T., C. P.; B., H. K.; Franck, E. U.; Datt, P.; Natu, V.; Pai, R.; Wilson, O.; Gadasu, E.; Badr, H.; Karmakar, A.; Magenau, A. J. D.; Kalra, V.; Barsoum, M. W.; Ando, Y.; Okubo, M.; Yamada, A.; Otani, M.; Osti, N. C.; Naguib, M.; Ganeshan, K.; Shin, Y. K.; Ostadhossein, A.; van Duin, A. C. T.; Cheng, Y.; Daemen, L. L.; Gogotsi, Y.; Mamontov, E.; Kolesnikov, A. I.; Berdiyorov, G. R.; Mahmoud, K. A.; Mertsoy, E. Y.; Zhang, X.; Cockreham, C. B.; Goncharov, V. G.; Guo, X.; Wang, J.; Wei, N.; Sun, H.; Wu, D.;

Levchenko, A. A.; Kolesnikov, A. I.; Trofymluk, O.; Navrotsky, A.; Costa, G. C. C.; McDonough, J. K.; Gogotsi, Y.; Navrotsky, A.; Shenderova, O.; Mochalin, V.; Gogotsi, Y.; Navrotsky, A.; Fredrickson, K. D.; Anasori, B.; Seh, Z. W.; Gogotsi, Y.; Vojvodic, A.; Pandey, M.; Thygesen, K. S.; Peng, Q.; Guo, J.; Zhang, Q.; Xiang, J.; Liu, B.; Zhou, A.; Liu, R.; Tian, Y.; Hu, T.; Hu, M.; Gao, B.; Li, W.; Wang, X. X.; Yang, D.; Zhao, C.; Lian, R.; Yang, L.; Wang, Y.; Gao, Y.; Xiao, X.; Gogotsi, Y.; Wang, X. X.; Chen, G.; Wei, Y. Y.; Björk, J.; Rosen, J.; Siriwardane, E. M. D.; Hu, J.; Shahzad, A.; Rasool, K.; Miran, W.; Nawaz, M.; Jang, J.; Mahmoud, K. A.; Lee, D. S.; Yu, Y.-X.; Srivastava, P.; Mishra, A.; Mizuseki, H.; Lee, K.-R.; Singh, A. K.; Ashton, M.; Mathew, K.; Hennig, R. G.; Sinnott, S. B.; Li, S.; Shi, Q.; Li, Y.; Yang, J.; Chang, T.-H.; Jiang, J.; Chen, P.-Y.; Gao, Q.; Sun, W.; Ilani-Kashkouli, P.; Tselev, A.; Kent, P. R. C.; Kabengi, N.; Naguib, M.; Alhabeb, M.; Tsai, W.-Y.; Baddorf, A. P.; Huang, J.; Jesse, S.; Gogotsi, Y.; Balke, N.; Ding, L.; Li, L.; Liu, Y.; Wu, Y.; Lu, Z.; Deng, J.; Wei, Y. Y.; Caro, J.; Wang, H.; Sun, Y.; Zhan, C.; Kent, P. R. C.; Naguib, M.; Gogotsi, Y.; Jiang, D.; Shpigel, N.; Chakraborty, A.; Malchik, F.; Bergman, G.; Nimkar, A.; Gavriel, B.; Turgeman, M.; Hong, C. N.; Lukatskaya, M. R.; Levi, M. D.; Gogotsi, Y.; Major, D. T.; Aurbach, D. Two-Dimensional Ti3C2Tx MXene Nanosheets for Efficient Copper Removal from Water. *J. Phys. Chem. C* **2021**, *120* (1), 2000820. https://doi.org/10.1021/acs.jpcc.8b04427.

(35) Li, J.; Wang, H.; Xiao, X.; Lu, M.; Han, W.; Li, H.; Zhang, W.; Zhang, B. There Is Plenty of Space in the MXene Layers: The Confinement and Fillings. *J. Energy Chem.* **2020**, *48* (3), 306–322. https://doi.org/10.1002/eem2.12090.

(36) Chen, H.; Ma, H.; Li, C. Host–Guest Intercalation Chemistry in MXenes and Its Implications for Practical Applications. *ACS Nano* **2021**, *15* (10), 15502–15537. https://doi.org/10.1021/acsnano.1c04423.

(37) Jiang, J.; Zou, Y.; Arramel; Li, F.; Wang, J.; Zou, J.; Li, N. Intercalation Engineering of MXenes towards Highly Efficient Photo(Electrocatalytic) Hydrogen Evolution Reactions. *J. Mater. Chem. A* **2021**, *9* (43), 24195–24214. https://doi.org/10.1039/D1TA07332J.

(38) Li, J.; Wang, H.; Xiao, X. Intercalation in Two-Dimensional Transition Metal Carbides and Nitrides (MXenes) toward Electrochemical Capacitor and Beyond. *ENERGY Environ. Mater.* **2020**, *3* (3), 306–322. https://doi.org/10.1002/eem2.12090.

(39) Fredrickson, K. D.; Anasori, B.; Seh, Z. W.; Gogotsi, Y.; Vojvodic, A. Effects of Applied Potential and Water Intercalation on the Surface Chemistry of Ti2C and Mo2C MXenes. *J. Phys. Chem. C* **2016**, *120* (50), 28432–28440. https://doi.org/10.1021/acs.jpcc.6b09109.

(40) Gao, Q.; Sun, W.; Ilani-Kashkouli, P.; Tselev, A.; Kent, P. R. C.; Kabengi, N.; Naguib, M.; Alhabeb, M.; Tsai, W.-Y.; Baddorf, A. P.; Huang, J.; Jesse, S.; Gogotsi, Y.; Balke, N. Tracking Ion Intercalation into Layered Ti3C2 MXene Films across Length Scales. *Energy Environ. Sci.* **2020**, *13* (8), 2549–2558. https://doi.org/10.1039/D0EE01580F.

(41) Sharma, G.; Muthuswamy, E.; Naguib, M.; Gogotsi, Y.; Navrotsky, A.; Wu, D. Calorimetric Study of Alkali Metal Ion (K+, Na+, Li+) Exchange in a Clay-Like MXene. *J. Phys. Chem. C* **2017**, *121* (28), 15145–15153. https://doi.org/10.1021/acs.jpcc.7b02419.

(42) Osti, N. C.; Naguib, M.; Ostadhossein, A.; Xie, Y.; Kent, P. R. C.; Dyatkin, B.; Rother, G.; Heller, W. T.; Van Duin, A. C. T.; Gogotsi, Y.; Mamontov, E. Effect of Metal Ion

Intercalation on the Structure of MXene and Water Dynamics on Its Internal Surfaces. *ACS Appl. Mater. Interfaces* **2016**, *8* (14), 8859–8863. https://doi.org/10.1021/acsami.6b01490.

(43) Overbury, S. H.; Kolesnikov, A. I.; Brown, G. M.; Zhang, Z.; Nair, G. S.; Sacci, R. L.; Lotfi, R.; van Duin, A. C. T.; Naguib, M. Complexity of Intercalation in MXenes: Destabilization of Urea by Two-Dimensional Titanium Carbide. *J. Am. Chem. Soc.* **2018**, *140* (32), 10305–10314. https://doi.org/10.1021/jacs.8b05913.

(44) Li, G.; Sun, H.; Xu, H.; Guo, X.; Wu, D. Probing the Energetics of Molecule-Material Interactions at Interfaces and in Nanopores. *J. Phys. Chem. C* **2017**, *121* (39). https://doi.org/10.1021/acs.jpcc.7b07450.

(45) Prescher, C.; Prakapenka, V. B. DIOPTAS: A Program for Reduction of Two-Dimensional X-Ray Diffraction Data and Data Exploration. *High Press. Res.* **2015**, *35* (3), 223–230. https://doi.org/10.1080/08957959.2015.1059835.

(46) Wang, H. W.; Naguib, M.; Page, K.; Wesolowski, D. J.; Gogotsi, Y. Resolving the Structure of Ti3C2Tx MXenes through Multilevel Structural Modeling of the Atomic Pair Distribution Function. *Chem. Mater.* **2016**, *28* (1), 349–359. https://doi.org/10.1021/acs.chemmater.5b04250.

(47) Doebelin, N.; Kleeberg, R. Profex: A Graphical User Interface for the Rietveld Refinement Program BGMN. *J. Appl. Crystallogr.* **2015**, *48*, 1573–1580. https://doi.org/10.1107/S1600576715014685.

(48) Graulis, S.; Chateigner, D.; Downs, R. T.; Yokochi, A. F. T.; Quirós, M.; Lutterotti, L.; Manakova, E.; Butkus, J.; Moeck, P.; Le Bail, A. Crystallography Open Database - An Open-Access Collection of Crystal Structures. *J. Appl. Crystallogr.* **2009**, *42* (4), 726–729. https://doi.org/10.1107/S0021889809016690.

(49) Gražulis, S.; Daškevič, A.; Merkys, A.; Chateigner, D.; Lutterotti, L.; Quirós, M.; Serebryanaya, N. R.; Moeck, P.; Downs, R. T.; Le Bail, A. Crystallography Open Database (COD): An Open-Access Collection of Crystal Structures and Platform for World-Wide Collaboration. *Nucleic Acids Res.* **2012**, *40* (D1), 420–427. https://doi.org/10.1093/nar/gkr900.

(50) Merkys, A.; Vaitkus, A.; Butkus, J.; Okulič-Kazarinas, M.; Kairys, V.; Gražulis, S. COD::CIF::Parser: An Error-Correcting CIF Parser for the Perl Language. *J. Appl. Crystallogr.* **2016**, *49*, 292–301. https://doi.org/10.1107/S1600576715022396.

(51) Quirós, M.; Gražulis, S.; Girdzijauskaitė, S.; Merkys, A.; Vaitkus, A. Using SMILES Strings for the Description of Chemical Connectivity in the Crystallography Open Database. *J. Cheminform.* **2018**, *10* (1), 1–17. https://doi.org/10.1186/s13321-018-0279-6.

(52) Vaitkus, A.; Merkys, A.; Grazulis, S. Validation of the Crystallography Open Database Using the Crystallographic Information Framework. *J. Appl. Crystallogr.* **2021**, *54*, 661–672. https://doi.org/10.1107/S1600576720016532.

(53) Jain, A.; Ong, S. P.; Hautier, G.; Chen, W.; Richards, W. D.; Dacek, S.; Cholia, S.; Gunter, D.; Skinner, D.; Ceder, G.; Persson, K. a. The Materials Project: A Materials Genome Approach to Accelerating Materials Innovation. *APL Mater.* **2013**, *1* (1), 11002.

https://doi.org/10.1063/1.4812323.

(54) Schneider, C. A.; Rasband, W. S.; Eliceiri, K. W. NIH Image to ImageJ: 25 Years of Image Analysis. *Nat. Methods* **2012**, *9* (7), 671–675. https://doi.org/10.1038/nmeth.2089.

(55) Navrotsky, A. Progress and New Directions in Calorimetry: A 2014 Perspective. *J. Am. Ceram. Soc.* **2014**, *97* (11), 3349–3359. https://doi.org/10.1111/jace.13278.

(56) Guo, X.; Boukhalfa, H.; Mitchell, J. N.; Ramos, M.; Gaunt, A. J.; Migliori, A.; Roback, R. C.; Navrotsky, A.; Xu, H. Sample Seal-and-Drop Device and Methodology for High Temperature Oxide Melt Solution Calorimetric Measurements of PuO2. *Rev. Sci. Instrum.* **2019**, *90* (4), 044101. https://doi.org/10.1063/1.5093567.

(57) Guo, X.; White, J. T.; Nelson, A. T.; Migdisov, A.; Roback, R.; Xu, H. Enthalpy of Formation of U3Si2: A High-Temperature Drop Calorimetry Study. *J. Nucl. Mater.* **2018**, *507*, 44–49. https://doi.org/10.1016/j.jnucmat.2018.04.032.

(58) Shpigel, N.; Chakraborty, A.; Malchik, F.; Bergman, G.; Nimkar, A.; Gavriel, B.; Turgeman, M.; Hong, C. N.; Lukatskaya, M. R.; Levi, M. D.; Gogotsi, Y.; Major, D. T.; Aurbach, D. Can Anions Be Inserted into MXene? *J. Am. Chem. Soc.* **2021**, *143* (32), 12552–12559. https://doi.org/10.1021/jacs.1c03840.

(59) Ren, C. E.; Hatzell, K. B.; Alhabeb, M.; Ling, Z.; Mahmoud, K. A.; Gogotsi, Y. Charge- and Size-Selective Ion Sieving Through Ti3C2Tx MXene Membranes. *J. Phys. Chem. Lett.* **2015**, *6* (20), 4026–4031. https://doi.org/10.1021/acs.jpclett.5b01895.

(60) Ding, L.; Li, L.; Liu, Y.; Wu, Y.; Lu, Z.; Deng, J.; Wei, Y.; Caro, J.; Wang, H. Effective Ion Sieving with Ti3C2Tx MXene Membranes for Production of Drinking Water from Seawater. *Nat. Sustain.* **2020**, *3* (4), 296–302. https://doi.org/10.1038/s41893-020-0474-0.

(61) Osti, N. C.; Naguib, M.; Ganeshan, K.; Shin, Y. K.; Ostadhossein, A.; van Duin, A. C. T.; Cheng, Y.; Daemen, L. L.; Gogotsi, Y.; Mamontov, E.; Kolesnikov, A. I. Influence of Metal Ions Intercalation on the Vibrational Dynamics of Water Confined between MXene Layers. *Phys. Rev. Mater.* **2017**, *1* (6), 65406. https://doi.org/10.1103/PhysRevMaterials.1.065406.

(62) Zheng, Z.; Guo, C.; Wang, E.; He, Z.; Liang, T.; Yang, T.; Hou, X. The Oxidation and Thermal Stability of Two-Dimensional Transition Metal Carbides and/or Carbonitrides (MXenes) and the Improvement Based on Their Surface State. *Inorg. Chem. Front.* **2021**, *8* (9), 2164–2182. https://doi.org/10.1039/D1QI00041A.

(63) Wenkui, G.; Ying, J.; Yongqin, L.; Delong, X.; Longbao, Z. Thermal Behavior of Aluminum Fluoride Trihydrate. *Thermochim. Acta* **2002**, *352–353*, 47–52. https://doi.org/10.1016/s0040-6031(99)00436-0.

(64) Dall'Agnese, C.; Dall'Agnese, Y.; Anasori, B.; Sugimoto, W.; Mori, S. Oxidized Ti3C2 MXene Nanosheets for Dye-Sensitized Solar Cells. *New J. Chem.* **2018**, *42* (20), 16446–16450. https://doi.org/10.1039/C8NJ03246G.

(65) Li, Z.; Wang, L.; Sun, D.; Zhang, Y.; Liu, B.; Hu, Q.; Zhou, A. Synthesis and Thermal Stability of Two-Dimensional Carbide MXene Ti3C2. *Mater. Sci. Eng. B Solid-State Mater. Adv. Technol.* **2015**, *191* (C), 33–40. https://doi.org/10.1016/j.mseb.2014.10.009.

(66) Levchenko, A. A.; Kolesnikov, A. I.; Trofymluk, O.; Navrotsky, A. Energetics of Single-Wall Carbon Nanotubes as Revealed by Calorimetry and Neutron Scattering. *Carbon N. Y.* **2011**, *49* (3), 949–954. https://doi.org/10.1016/j.carbon.2010.11.004.

(67) Costa, G. C. C.; McDonough, J. K.; Gogotsi, Y.; Navrotsky, A. Thermochemistry of Onion-like Carbons. *Carbon N. Y.* **2014**, *69*, 490–494. https://doi.org/10.1016/j.carbon.2013.12.053.

(68) Costa, G. C. C.; Shenderova, O.; Mochalin, V.; Gogotsi, Y.; Navrotsky, A. Thermochemistry of Nanodiamond Terminated by Oxygen Containing Functional Groups. *Carbon N. Y.* **2014**, *80* (1), 544–550. https://doi.org/10.1016/j.carbon.2014.08.094.

(69) Mertsoy, E. Y.; Zhang, X.; Cockreham, C. B.; Goncharov, V. G.; Guo, X.; Wang, J.; Wei, N.; Sun, H.; Wu, D. Thermodynamic, Thermal, and Structural Stability of Bimetallic MIL-53 (Al1–XCrx). *J. Phys. Chem. C* **2021**, *125* (25), 14039–14047. https://doi.org/10.1021/acs.jpcc.1c02623.

(70) Nam, K. M.; Shim, J. H.; Han, D.-W.; Kwon, H. S.; Kang, Y.-M.; Li, Y.; Song, H.; Seo, W. S.; Park, J. T. Syntheses and Characterization of Wurtzite CoO, Rocksalt CoO, and Spinel Co3O4 Nanocrystals: Their Interconversion and Tuning of Phase and Morphology. *Chem. Mater.* **2010**, *22* (15), 4446–4454. https://doi.org/10.1021/cm101138h.

(71) Nordin, E.; Rafstedt, J. L. Evaluation of the Drying Process at Alufluor AB, Lund University, 2017.

(72) Domalski, E. S.; Armstrong, G. T. Heat of Formation of Aluminum Fluoride by Direct Combination of the Elements. *J. Res. Natl. Bur. Stand. Sect. A, Phys. Chem.* **1965**, *69A* (2), 137–147. https://doi.org/10.6028/jres.069A.016.

(73) Berdiyorov, G. R.; Mahmoud, K. A. Effect of Surface Termination on Ion Intercalation Selectivity of Bilayer Ti3C2T2 (T=F, O and OH) MXene. *Appl. Surf. Sci.* **2017**, *416*, 725–730. https://doi.org/10.1016/j.apsusc.2017.04.195.

(74) Liu, J.; Zhang, H.-B.; Sun, R.; Liu, Y.; Liu, Z.; Zhou, A.; Yu, Z.-Z. Hydrophobic, Flexible, and Lightweight MXene Foams for High-Performance Electromagnetic-Interference Shielding. *Adv. Mater.* **2017**, *29* (38), 1702367. https://doi.org/10.1002/adma.201702367.

(75) Zhou, H.; Wang, F.; Wang, Y.; Li, C.; Shi, C.; Liu, Y.; Ling, Z. Study on Contact Angles and Surface Energy of MXene Films. *RSC Adv.* **2021**, *11* (10), 5512–5520. https://doi.org/10.1039/D0RA09125A.

(76) Fard, A. K.; Mckay, G.; Chamoun, R.; Rhadfi, T.; Preud'Homme, H.; Atieh, M. A. Barium Removal from Synthetic Natural and Produced Water Using MXene as Two Dimensional (2-D) Nanosheet Adsorbent. *Chem. Eng. J.* **2017**, *317*, 331–342. https://doi.org/10.1016/j.cej.2017.02.090.

(77) Yang, J.; Bao, W.; Jaumaux, P.; Zhang, S.; Wang, C.; Wang, G. MXene-Based Composites: Synthesis and Applications in Rechargeable Batteries and Supercapacitors. *Adv. Mater. Interfaces* **2019**, *6* (8), 1–32. https://doi.org/10.1002/admi.201802004.

(78) Natu, V.; Pai, R.; Wilson, O.; Gadasu, E.; Badr, H.; Karmakar, A.; Magenau, A. J. D.; Kalra, V.; Barsoum, M. W. Effect of Base/Nucleophile Treatment on Interlayer Ion Intercalation,

Surface Terminations, and Osmotic Swelling of Ti3C2Tz MXene Multilayers. *Chem. Mater.* **2022**, *34* (2), 678–693. https://doi.org/10.1021/acs.chemmater.1c03390.

(79) Seredych, M.; Shuck, C. E.; Pinto, D.; Alhabeb, M.; Precetti, E.; Deysher, G.; Anasori, B.; Kurra, N.; Gogotsi, Y. High-Temperature Behavior and Surface Chemistry of Carbide MXenes Studied by Thermal Analysis. *Chem. Mater.* **2019**, acs.chemmater.9b00397. https://doi.org/10.1021/acs.chemmater.9b00397.

(80) Levchenko, A. A.; Li, G.; Boerio-Goates, J.; Woodfield, B. F.; Navrotsky, A. TiO2 Stability Landscape: Polymorphism, Surface Energy, and Bound Water Energetics. *Chem. Mater.* **2006**, *18* (26), 6324–6332. https://doi.org/10.1021/cm061183c.

(81) Wen, J.; Zhang, X.; Gao, H. Role of the H-Containing Groups on the Structural Dynamics of Ti3C2Tx MXene. *Phys. B Condens. Matter* **2018**, *537*, 155–161. https://doi.org/10.1016/j.physb.2018.02.012.

(82) Gokel, G. W. 1.01 - Introduction and Overview of Supramolecular Receptor Types; Atwood, J. L. B. T.-C. S. C. I. I., Ed.; Elsevier: Oxford, 2017; pp 1–10. https://doi.org/https://doi.org/10.1016/B978-0-12-409547-2.12472-2.

(83) Roy, K.; Kar, S.; Das, R. N. Chapter 1 - Background of QSAR and Historical Developments; Roy, K., Kar, S., Das, R. N. B. T.-U. the B. of Q. for A. in P. S. and R. A., Eds.; Academic Press: Boston, 2015; pp 1–46. https://doi.org/https://doi.org/10.1016/B978-0-12-801505-6.00001-6.

(84) Levchenko, A. A.; Kolesnikov, A. I.; Ross, N. L.; Boerio-Goates, J.; Woodfield, B. F.; Li, G.; Navrotsky, A. Dynamics of Water Confined on a TiO2 (Anatase) Surface. *J. Phys. Chem. A* **2007**, *111* (49), 12584–12588. https://doi.org/10.1021/jp076033j.

(85) Spencer, E. C.; Levchenko, A. A.; Ross, N. L.; Kolesnikov, A. I.; Boerio-Goates, J.; Woodfield, B. F.; Navrotsky, A.; Li, G. Inelastic Neutron Scattering Study of Confined Surface Water on Rutile Nanoparticles. *J. Phys. Chem. A* **2009**, *113* (12), 2796–2800. https://doi.org/10.1021/jp8109918.

(86) Li, S.; Shi, Q.; Li, Y.; Yang, J.; Chang, T.-H.; Jiang, J.; Chen, P.-Y. Intercalation of Metal Ions into Ti3C2Tx MXene Electrodes for High-Areal-Capacitance Microsupercapacitors with Neutral Multivalent Electrolytes. *Adv. Funct. Mater.* **2020**, *30* (40), 2003721. https://doi.org/10.1002/adfm.202003721.

(87) Anasori, B.; Xie, Y.; Beidaghi, M.; Lu, J.; Hosler, B. C.; Hultman, L.; Kent, P. R. C.; Gogotsi, Y.; Barsoum, M. W. Two-Dimensional, Ordered, Double Transition Metals Carbides (MXenes). *ACS Nano* **2015**, *9* (10), 9507–9516. https://doi.org/10.1021/acsnano.5b03591.

(88) Zhang, N.; Hong, Y.; Yazdanparast, S.; Asle Zaeem, M. Superior Structural, Elastic and Electronic Properties of 2D Titanium Nitride MXenes over Carbide MXenes: A Comprehensive First Principles Study. *2D Mater.* **2018**, *5* (4), 45004. https://doi.org/10.1088/2053-1583/aacfb3.